International Institute for Applied Systems Analysis
IIASA www.iiasa.ac.at

Address: IIASA, Schlossplatz 1, A-2361 Laxenburg, Austria

Email: permissions@iiasa.ac.at

Report

Full of Economic-Environment Linkages and Integration dX/dt (FeliX)

Technical Model Documentation

Sibel Eker, eker@iiasa.ac.at

Qi Liu, liu@iiasa.ac.at

Claudia Reiter, reiter@iiasa.ac.at

Michael Kuhn, kuhn@iiasa.ac.at

August 2023

Table of contents

ZVR 524808900

Disclaimer, funding acknowledgment, and copyright information:

IIASA Reports report on research carried out at IIASA and have received only limited review. Views or opinions expressed herein do not necessarily represent those of the institute, its National Member Organizations, or other organizations supporting the work.

The authors gratefully acknowledge funding from the European Research Council for the research project 'The Demography of Sustainable Human Wellbeing' (ERC-2016-ADG, Grant agreement ID 741105).

Abstract

FeliX is a global system dynamics model of climate, economy, environment and society. The FeliX model has been extended recently to analyze the future dynamics of global wellbeing, indicated by the novel Years of Good Life (YoGL) metric, with respect to the interactions between global demographics, climate change, economic growth and environmental change. This technical report documents the population, economy and wellbeing modules of the FeliX model relevant for formulating global wellbeing. In addition to the model description, the report includes a detailed explanation of the baseline scenarios used for exploring global wellbeing dynamics. This document is complementary to the main publications that present the global integrated wellbeing analysis using the FeliX model, including the IIIASA Flagship Report (2023), and can be referred to as a technical guide.

About the authors

Sibel Eker is a Research Scholar at IIASA's Energy, Climate and Environment Program, and an Assistant Professor at Radboud University, Netherlands. (Contact: eker@iiasa.ac.at)

Qi Liu is a Researcher at Sichuan University, China, and a Guest Research Scholar at IIASA's Economic Frontiers Program. (Contact: liuqi@iiasa.ac.at; liuqi_67@stu.scu.edu.cn)

Claudia Reiter is a Researcher at the Institute for Advanced Studies Vienna, a Researcher and Lecturer at University of Vienna, and a Guest Research Scholar at IIASA's Economic Frontiers Program (Contact: reiter@iiasa.ac.at)

Michael Kuhn is Director of the Economic Frontiers Program, and Principal Research Scholar at IIASA. (Contact: kuhn@iiasa.ac.at)

Acknowledgments

We are grateful to Wolfgang Lutz, Warren Sanderson and Shonali Pachauri for their comments on the model scope and outcomes, and to all IIASA colleagues who participated in the FeliX review and wellbeing modelling workshop held in March 2023.

1. Introduction and Model Overview

Global modelling has long been an indispensable tool for understanding the interdependencies between social, economic, and environmental systems and exploring plausible future dynamics created by those[1]. FeliX is one of such models developed at IIASA first in 2006-2009 to support global earth observations within the GEO-BENE project funded by the European Commission. It is a globally aggregate, feedback-rich simulation model of climate, economy, environment, and society. FeliX has been used in various projects since then, for instance, to assess the socio-economic and environmental impacts of earth observation improvement[2,3], to explore emission pathways when microalgae is used as a feedstock in livestock production[4], and to analyze carbon cycle impacts of global emission pathways[5], and population dynamics of shifts to sustainable diets[6]. The feedback-rich broad scope of FeliX has also enabled analyzing synergies and tradeoffs between sustainable development goals (SDGs) in long-term pathways beyond 2030[7], and specifically the tradeoffs between environmental pressures and eradicating global poverty[8].

The FeliX model captures the core physical and anthropogenic mechanisms of global environmental and economic change within and between population, economy, energy, carbon cycle, climate, biodiversity, water, and land use. Figure 1 shows an overview of the main sectors in the model and their interconnections. Those cross-sectorial interconnections include the major human-earth system feedbacks, such as climate impacts on economic growth, crop yields, and human mortality or the impacts of economic growth on population dynamics, which are not endogenously covered in many global models.

A recent extension of the FeliX incorporated a measure of human wellbeing, indicated by Years of Good Life (YoGL) metric, in relation to demographic, economic and environmental factors. This report provides a documentation of this wellbeing module of the FeliX model, as well as the tightly related economy and population sectors. In addition to the description of these model sectors in Sections 2-4, Section 5 presents a **complementary** description of the scenario analysis conducted in the context of global wellbeing (as published in the IIASA Flagship Report, 2023). The documentation of the other model sectors can be found in the following sources:

- Energy, biodiversity, water: Rydzak et al.[9]
- Carbon cycle and climate: Walsh et al.[5] (Methods)
- Land use, food demand and supply, fertilizer consumption: Eker et al.[6] (Methods and Supplementary Information) & Moallemi et al.[7] (Methods and Supplementary Information)

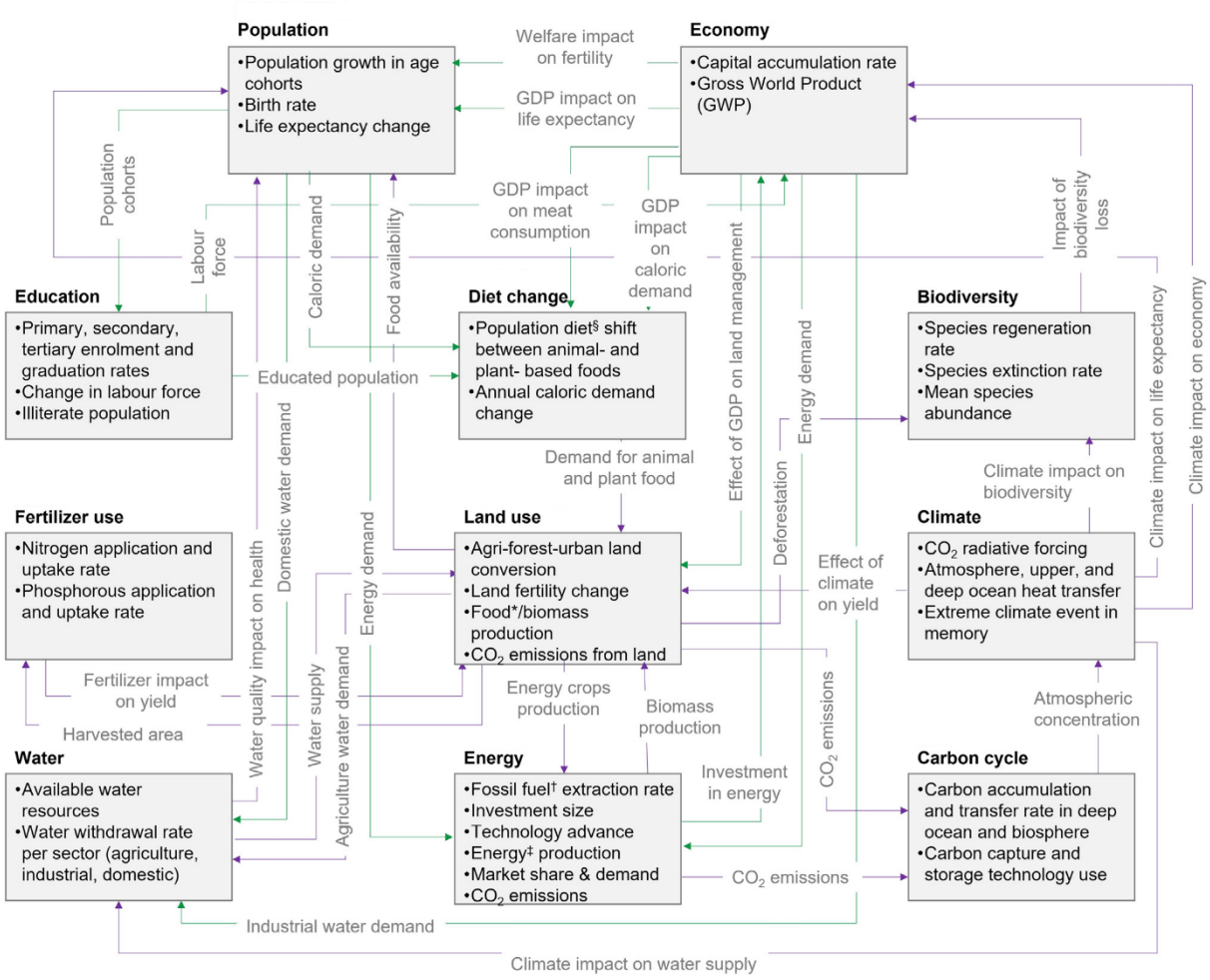

Figure 1: Overview of the FeliX model. Source: Moallemi et al. (2022)

2. Population

The FeliX model has an endogenous population module that was conceptualized around two main dynamic mechanisms: population development and population ageing. Population development is governed by two key feedback loops visualized in Figure 2. The positive feedback loop describes the population growth mechanism:

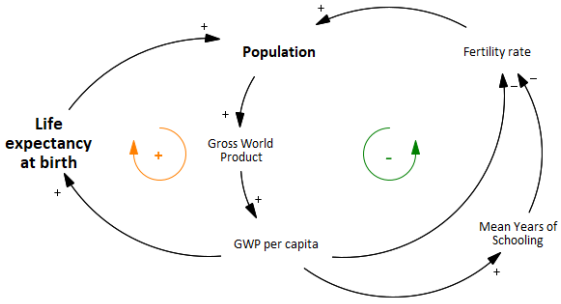

Figure 2: Main feedback loops in the population module

A growing *Population* leads to a higher economic output expressed in *Gross World Product (GWP) per capita*. This economic growth increases the *life expectancy at birth*, reduces mortality, and hence further increases the population. The two negative feedback loops describe the balancing effect of economic growth on population: *Fertility rates* decline as *GWP per capita* and educational attainment (expressed in the *Mean Years of Schooling* metric) increase. The population module connects several cross-system feedback loops, for instance through the effect of food supply per capita or climate change on life expectancy, or through the effects of educational attainment on dietary behavior and poverty rate. The sections below describe how the population module is formalized in the FeliX model.

2.1. Ageing structure

This module describes population growth and population ageing based on an ageing chain and computes the male and female population size of 5-year age intervals between the ages of 0 and 100+. The chain structure in the model represents the transition of newborns through the age cohorts as they age, meaning that each age cohort except the "0–5" cohort has one inflow (maturation of the previous cohort) and two outflows (maturation to the next cohort and mortality). Figure 3 depicts this ageing chain, and the implementation of it on Vensim uses a compact form with subscripts. *Population* of each gender and age interval ($Population_{ij}$) is conceptualized in a stock variable that represents the accumulations, with three flows determining the net rate of change ($dPopulation_{ij}/dt$). These three flows are *birth rate* ($Birth_{ij}$), death rate ($Death_{ij}$) and maturation rate ($Maturation_{ij}$). Equation 2.1 shows the formulation of this net rate of change in the population depending on the age intervals, where the index ***i* refers to gender and *j* refers to age**. The maturation rate of each age group, that is, the transition to the next age interval, is formulated as the division of *Population* by the interval duration as in Equation 2.2, assuming a homogenous distribution of population within the age group. *Interval duration* is a parameter equal to 5 years.

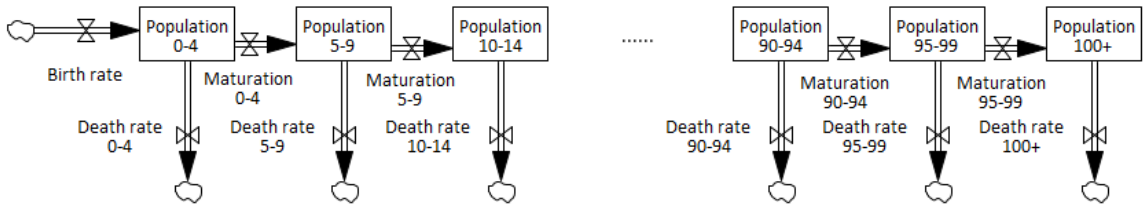

Figure 3: Ageing chain structure of the population module

$$\frac{dPopulation_{ij}(t)}{dt} = \begin{cases} Birth_i(t) - Maturation_{ij}(t) - Death_{ij}(t) \;\; ; if \;\; j = "0-4" \\ Maturation_{ij-1}(t) - Maturation_{ij}(t) - Death_{ij}(t) \;\; ; \;\; if \; "5\text{-}9" \leq j \leq "95\text{-}99" \\ Maturation_{ij-1}(t) - Death_{ij}(t) \;\; ; \;\; if \; j = "100+" \end{cases} \quad (2.1)$$

$$Maturation_{ij}(t) = \frac{Population_{i,}(t)}{Interval\ duration} \quad (2.2)$$

2.2. Birth rate and fertility

The birth rate[1], driven by education and gross domestic product (GDP) per capita, is the main factor affecting population dynamics (either growth or decline), alongside the reproductive female population represented by gender and age-cohort segmentation in the model. Equation 2.3 shows the formulation of *birth rate* per year, where the parameter g_i denotes the birth gender fraction, hence female infanticide, and the parameter *age interval duration* is 5 years. The numerator in the equation refers to the total births in a 5-year interval, formulated as the sum of births for women in each 5-year age interval between 15 and 50. $ASFR_j$ refers to the *Age-Specific Fertility Rate*, that is, number of births per woman in a particular age group during a five-year period. *ASFR* is formulated as a function of *Total Fertility* as shown in Equation 2.4, in order to take the effects of education and wealth on fertility into account in an aggregate manner. The functions representing the relationship between *ASFR* and *Total Fertility* are formulated as logistic functions and estimated based on historical relationships (including SSP2 projections) obtained from the Wittgenstein Centre Human Capital Data Explorer, as shown in Figure 4.

$$Birth_i(t) = g_i \times \frac{\sum_{j=15-19}^{45-49} Population_{female,j}(t) \times ASFR_j(t)}{Age\ interval\ duration} \quad (2.3)$$

$$ASFR_j(t) = f_j^{asfr}\big(Total\ Fertility(t)\big) \quad (2.4)$$

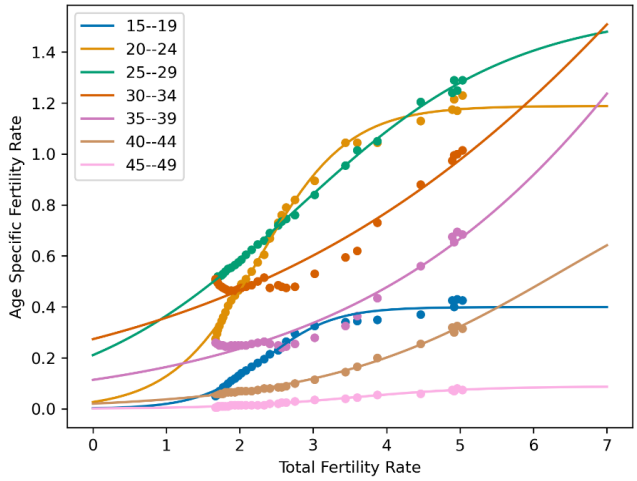

Age	R2
15--19	0.983
20--24	0.994
25--29	0.999
30--34	0.935
35--39	0.948
40--44	0.996
45--49	0.986

Figure 4: Relationship between Age-Specific Fertility Rate and Total Fertility. Dots refer to the N=30 historical data points SSP2 projections in 5-year intervals between 1955-2100 obtained from Wittgenstein Centre Human Capital Data Explorer. The lines show the logistic curve (f^{asfr}) fit to the historical data for each age interval in the reproductive period, and the right-hand-side table shows the R-squared values of the fitted curves.

[1] In system dynamics modelling, the term *rate* refers to the rate of change in a stock variable, that is, a flow. Therefore, here we use the term *rate* to refer to the flows, not to the fractions as used in demography.

Total Fertility represents the number of births per woman at reproductive age (15-50). It is formulated as a multiplicative function of *GWP per capita* and *Mean Years of Schooling (MYS)*. This formulation prevents a strong assumption on the monotonic dependence of fertility solely on economic output or solely on education. Equation 2.5 shows this formulation, where *Normal Fertility* is the reference value equal to the historical value in year 2000, which is 2.63 births per woman.

$$Total\ Fertility(t) = Normal\ Fertility \times Impact_{fertility}^{education}(t) \times Impact_{fertility}^{GDP}(t) \quad (2.5)$$

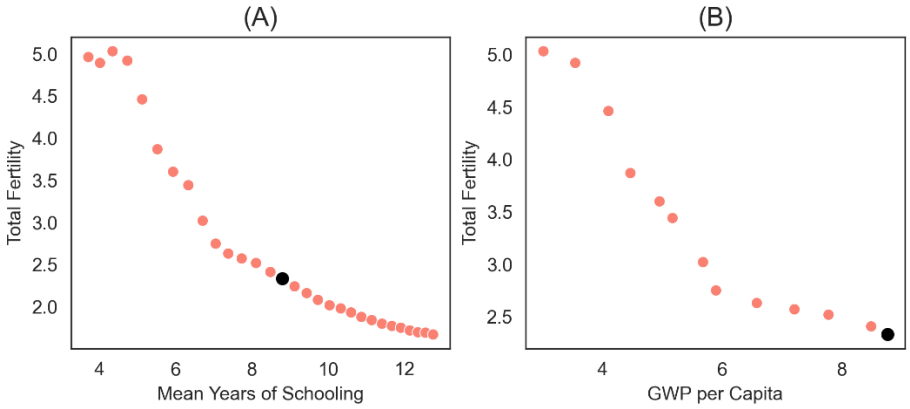

Figure 5: Observed relationship between fertility rate and its two drivers: **(A)** The relationship between the global average Total Fertility Rate (births per woman at the reproductive age) and Mean Years of Schooling based on the historical data of 1950-2015 and SSP2 projections for 2015-2100 of Wittgenstein Centre Human Capital Data Explorer[10]. **(B)** The relationship between the global average Total Fertility Rate and the GWP per Capita between the years 1960-2020. GWP per Capita is measured in 1000 USD 2005 PPP and obtained from World Bank data[11]. The black dot shows the 2020 values.

Impact of Education on Fertility ($Impact_{fertility}^{education}$) is a nonlinear function that depends on global average *Mean Years of Schooling* (*MYS*) as formulated in Equation 2.6. In this formula, *L, k and* x_0 refer to the saturation, steepness and inflection point of the logistic curve, respectively. *MYS** is a normalized form of the model variable *Mean Years of Schooling,* that is, $MYS(t)/MYS_{2000}$, in order to make both Total Fertility and its drivers variable with respect to their values in year 2000. A functional form representing logarithmic decline is chosen, following the the observed MYS-fertility relationship shown in Figure 5a. Similarly, *Impact of GDP on Fertility* ($Impact_{fertility}^{GDP}$) is a nonlinear (logistic) function that depends on *Gross World Product (GWP) per Capita* as formulated in Equation 2.7. This function form is chosen to represent the observed GDP-fertility relationship shown in Figure 5b. *GWP per Capita** is a normalized form of the model variable *GWP per Capita,* that is, $GWP\ per\ Capita(t)/GWP\ per\ Capita_{2000}$.

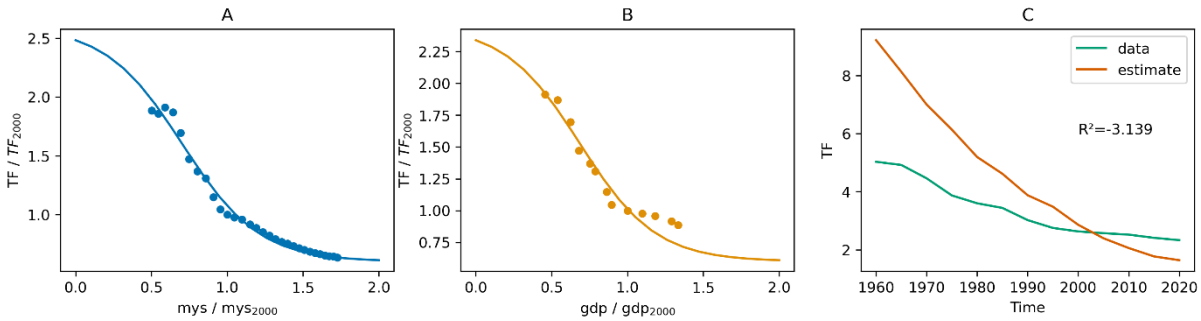

Figure 6: Step 1 of the calibration of the relations between Total Fertility and MYS and GWP per Capita. **(A)** The relationship between normalized Total Fertility Rate (y-axis) and normalized Mean Years of Schooling (x-axis). The dots refer to the historical data of 1950-2015 and SSP2 projections for 2015-2100 of Wittgenstein Centre Human Capital Data Explorer[10]. The line shows the logistic curve fitted to these data with R^2=0.985. **(B)** The relationship between normalized Total Fertility Rate (y-axis) and normalized GWP per Capita (x-axis). The dots refer to the historical data between 1960-2020 obtained from World Bank data[11]. The line shows the logistic curve fitted to these data with R^2=0.932. **(C)** Total Fertility rate over time as observed in historical data (green line) and as estimated according to Equation (2.5) and calibrated functions shown in (A) and (B).

$$Impact_{fertility}^{education}(t) = L_{0,edu} + \frac{L_{fer}^{edu}}{1 + e^{-k_{fer}^{edu} \times \left(MYS^*(t) - x0_{fer}^{edu}\right)}} \tag{2.6}$$

$$Impact_{fertility}^{GDP}(t) = L_{0,gdp} + \frac{L_{fer}^{gdp}}{1 + e^{-k_{fer}^{gdp} \times \left(GWP\ per\ Capita^*(t) - x0_{fer}^{gdp}\right)}} \tag{2.7}$$

Figure 6a and Figure 6b show the model functions denoted in Equations 2.6 and 2.7, respectively, of which parameters are calibrated according to the historical values. Since these *Step 1* calibrations do not take the joint effect of MYS and GWP into account, the resulting *Total Fertility* is far different from the observed values, as Figure 6c shows. To take the joint effect into account with a lower degree of freedom, we keep the parameters representing steepness and inflection of these functions (k_{edu}, $x_{0,edu}$, k_{gdp}, $x_{0,gdp}$) at the values obtained from the regression in Step 1 and re-calibrate the parameters representing the scale of the impacts (L_{edu} and L_{gdp}) to the historical values of total fertility. The resulting estimate of *Total Fertility* is shown in Figure 7c, and the updated functional forms of the impact of education and GDP are shown in Figure 7a and Figure 7b, respectively. These constitute the final model functions.

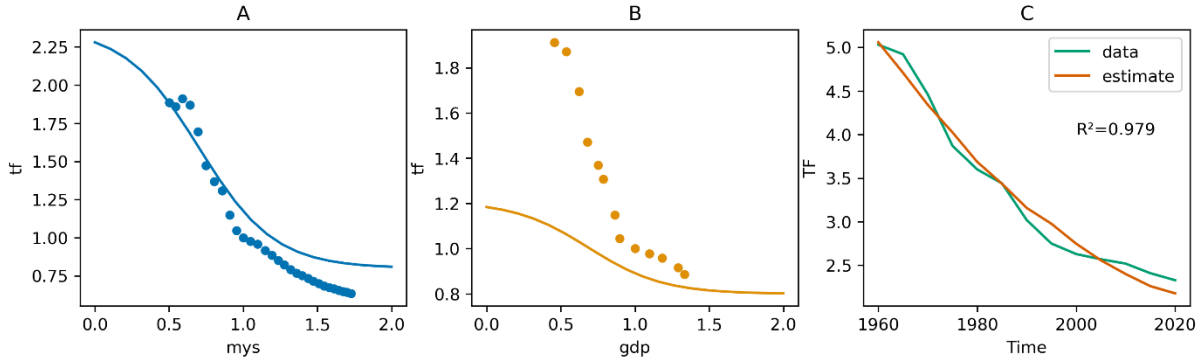

Figure 7: Step 2 of the calibration of the relations between Total Fertility and MYS and GWP per Capita. **(A and B)** The relationship between normalized Total Fertility Rate (y-axis) and normalized Mean Years of Schooling (x-axis, A) and normalized GWP per Capita (x-axis, B), respectively. The dots refer to the historical data. The lines show the logistic curve resulting from the fit of the parameters L_{edu} and L_{gdp}, whereas the other parameters are kept at the values obtained in Step 1 (Figure 6). **(C)** Total Fertility rate over time as observed in historical data (green line) and as estimated according to Equation (2.5) and calibrated functions shown in (A) and (B).

Based on the functional forms and calibration described above, the reference simulation of the model generates the trajectories for global average *Total Fertility* and *global Total Birth Rate* shown in Figure 8.

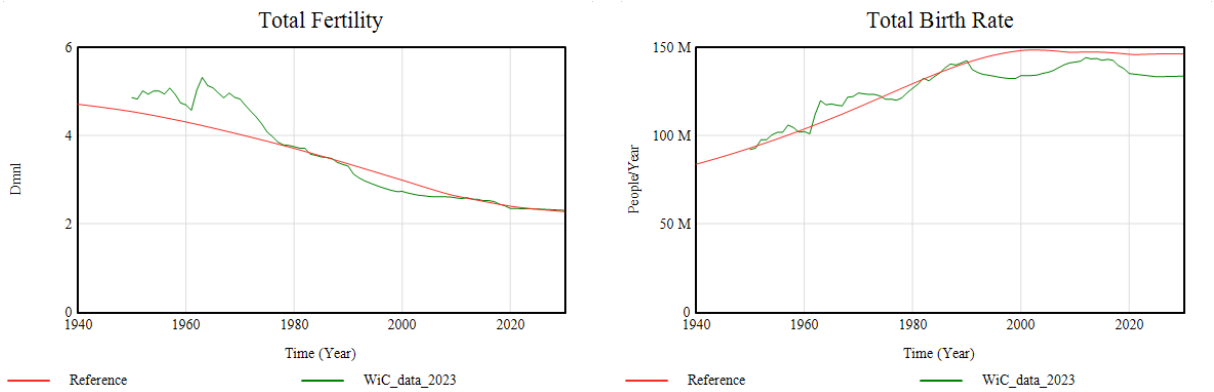

Figure 8: Reference simulation results (BAU, red line) and historical data (Data, green line) of Total Fertility and Total Birth Rate. The data for Total Fertility is obtained from Wittgenstein Centre Human Capital Data Explorer[10]. The data for Total Birth Rate is obtained from UN Population Prospects[12].

2.3. Mortality rate and life expectancy at birth

Death rate (*Death*$_{ij}$) refers to the number of people who pass away in each demographic gender and age group per year. It is formulated as a fraction of the population of each group as Equation 2.8 shows, where *M*$_{ij,}$ denotes the mortality fraction. The mortality fraction for each age and gender group is assumed to be a function of global average life expectancy at birth (*LE*) (Equation 2.9). This assumption reflects the relationship between life expectancy and wider socioeconomic and environmental factors, such as education, wealth, climate change, aggregately; and, in turn, their relationship with mortality rates.

$$Death_{ij}(t) = Population_{ij}(t) \times M_{ij}(t) \quad (2.8)$$

$$M_{ij}(t) = Mor_{ij}(t) + \left(\frac{L\,mor_{ij}}{1 + e^{\left(-K\,mor_{i,j} \times \left(\frac{LE(t)}{LE^*} - x_0\,mor_{ij}\right)\right)}}\right) \quad (2.9)$$

LE* is a reference value of life expectancy at birth used for normalization, and currently 28.8, referring to the values at the beginning of the 20th century. Mor_{ij}, $L\,mor_{ij}$, $K\,mor_{ij}$, and $x_0\,mor_{ij}$ are parameters obtained by the model calibration of mortality fractions. The model calibration of mortality fractions is conducted by fitting the model simulation results and historical data of each gender and age group. The historical data of the mortality fraction of each gender and age group is collected from UN Population Prospects[12]. Figure 9 shows the calibration results for the mortality fraction of each gender and age group, and Table 1 lists the R^2 values of the fit between the model output and historical data (including UN projections until 2100). It is important to note that climate impacts on mortality are not taken into account in this calibration, since the projections do not include it either.

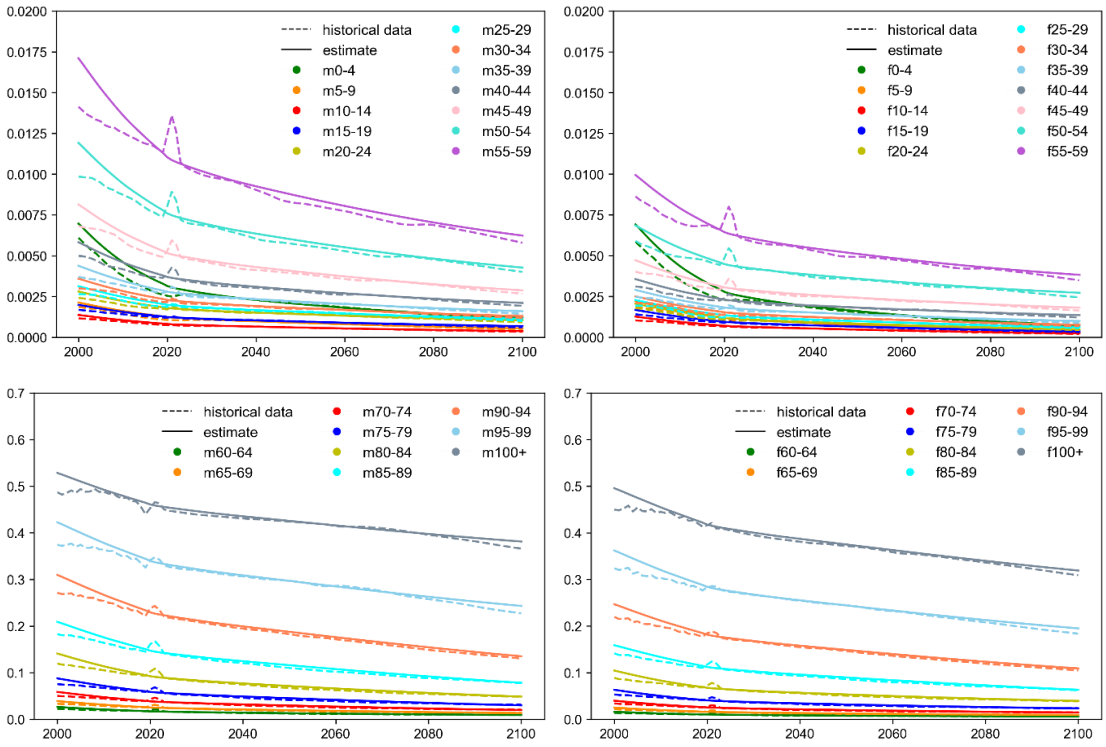

Figure 9: Calibration results of mortality fractions of different age groups excluding climate impacts on mortality. "m" and "f" indicate male and female, respectively. The source of historical data (including projections) is UN Population Prospects[12].

Table 1: R^2 for the estimated values and historical data of mortality fractions grouped by gender and age (excluding climate impacts on mortality).

R^2	Male	Female
0-4	0.9995	0.9998
5-9	0.9997	0.9996
10-14	0.9998	0.9995
15-19	0.9995	0.9995
20-24	0.9995	0.9998
25-29	0.9996	0.9997
30-34	0.9996	0.9997
35-39	0.9994	0.9995
40-44	0.9993	0.9993
45-49	0.9992	0.9991
50-54	0.9989	0.9987
55-59	0.9977	0.9986
60-64	0.9965	0.9984
65-69	0.9958	0.9987
70-74	0.9949	0.9988
75-79	0.9938	0.9988
80-84	0.9965	0.9989
85-89	0.9916	0.9949
90-94	0.9932	0.9952
95-99	0.9910	0.9934
100+	0.9895	0.9912

Life Expectancy at Birth (LE) is obtained by a multiplicative function of the impacts of *GDP per Capita*, *Mean Years of Schooling*, *Total Food Supply per Capita,* and climate change on a reference value of LE, that is, the observed life expectancy at birth in year 2000 (LE_{2000}) (Equation 2.(2.10)). Each of these functions are assumed to follow a logistic function formulation which yields a flexible function form, e.g. pseudo-linear, depending on parameterization, as stated in Equation 2.(2.11). Similar to the calibration of *Total Fertility* described in Section 2.2, these multiple impacts on life expectancy are calibrated in a step-wise manner. First, the impact of each driver is calibrated, as if it were the sole factor affecting life expectancy, as exemplified in Figure 10. Then, the parameters x_0 are kept constant at their calibrated values, and the other parameters that define the scale and steepness of the function are varied to calibrate the joint impact of drivers. The resulting functions can be seen in Figure 11.

$$LE(t) = LE_{2000} \times Impact_{le}^{gdp}(t) \times Impact_{le}^{mys}(t) \times Impact_{le}^{food}(t) \times Impact_{le}^{climate}(t) \quad (2.10)$$

$$Impact_{le}^{gdp}(t) = \frac{L_{le}^{gdp}}{1 + e^{-k_{le}^{gdp} \times \left(GWP\ per\ Capita^{*}(t) - x0_{le}^{gdp}\right)}} \quad (2.11)$$

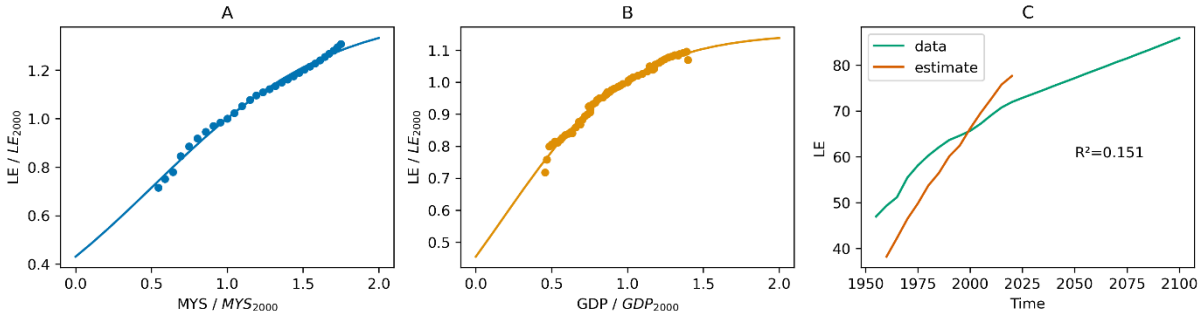

Figure 10: Initial calibration of the drivers of life expectancy at birth. In panels A and B, the dots refer to the historical data obtained from Wittgenstein Center for Data Explored (MYS and Life Expectancy), and from World Bank statistics (GDP per capita). Lines refer to the calibrated function.

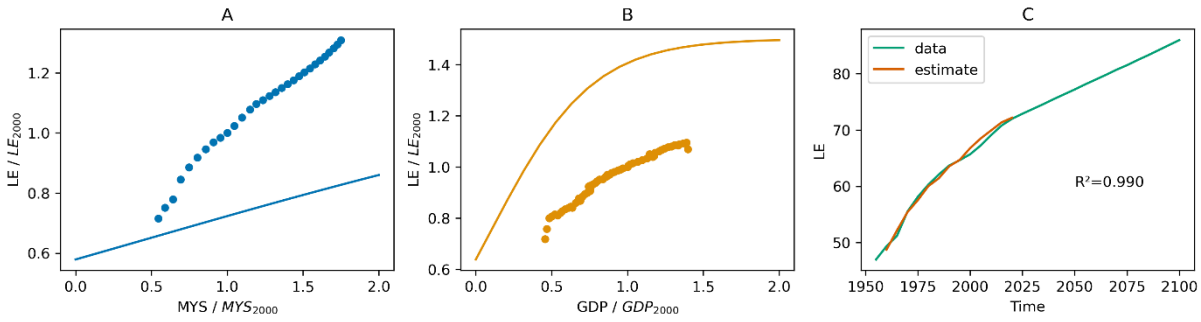

Figure 11: Final calibration of the impacts of education and economic growth on life expectancy at birth.

The impact of food supply on life expectancy ($Impact_{le}^{food}$) is formulated and calibrated similarly, taking the impacts of education and economic growth into account. Figure 12a shows the historical and model-generated relationship between Life Expectancy at Birth and Total Food Supply per Capita in the period 1960-2020, and Figure 12b depicts the multiplier function $Impact_{le}^{food}$ calibrated to this historical data while taking the impacts of education and economic growth into account.

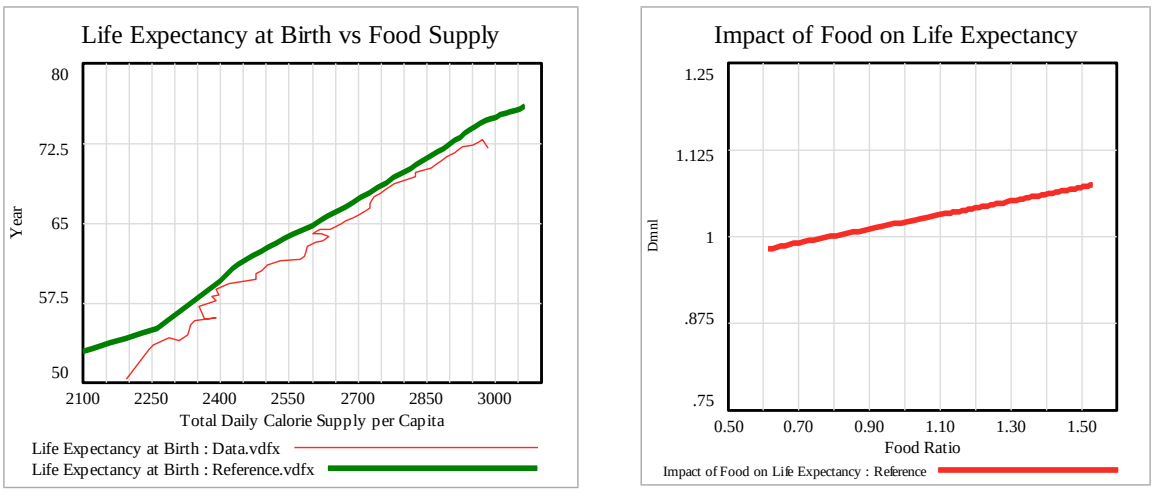

(a) (b)

Figure 12: Impact of food supply on life expectancy. In (a), the red line shows the historical values of global average Life Expectancy at Birth (obtained from [10]) and Total Daily Caloric Food Supply per Capita (obtained from UN FAO Food Balance Sheets[14]). The green line shows the simulation results in the reference scenario. In (b), the impact of food supply on life expectancy, as a multiplier, can be seen, where the x-axis shows the ratio of total daily caloric food supply per capita to the subsistence caloric value, which 2000 kcal per day per person.

The last driver of life expectancy modeled in FeliX is the impact of climate change ($Impact_{le}^{climate}$). Since most of the impact is expected to be observed in future, we did not include it in the calibration to historical data, but we used the temperature-dependent estimates for future projections. Global temperature rise is the main driver of climate mortality, yet those impacts are expected to be mediated by education, therefore we used a formulation that takes both factors into account and calibrated it to the estimates of Bressler et al. (2021)[13] for climate impacts on mortality.

The impact of climate change on life expectancy is inversely proportional to the impact of climate on the mortality fraction ($Impact_{mor}^{climate}$), as shown in Equation 2.12, assuming that global average mortality fraction is equal to $1/LE$. Bressler et al. (2021)[13] estimate the climate impacts on mortality for a 0 – 4 °C increase in global temperature as compared to 2000-2019 levels. To account for temperature rise beyond this range, we first estimate the impact of temperature change on mortality based on a multivariate regression model, where we control for educational attainment in line with evidence on its role in terms of adaptive capacity[15,16]. Based on this model, we predict the mortality impact using a range of different values for both temperature change and education. In a next step, and to account for the nonlinearities, we use a logistic function as a proxy for this temperature – mortality impact function (Equation 2.13) and calibrate it to the estimates for the 0-5 °C temperature increase compared to preindustrial times (Figure 13a). This results in the parameter values 7.96, 0.68, 7.76 for y_{mor}, L_{mor}, and $x_{0,mor}$, respectively. In line with the literature and drawing on our regression predictions, we assume that the steepness of this function (k_{mor}) represents the impact of education. As Equation 2.14 shows, we implement two alternative formulations for k_{mor}, depending on *mean years of schooling* (MYS) or the *share of females aged 20-39 with minimum secondary education* (*FE*), respectively. While the former is a widely used summary measure for human capital, the latter was chosen as an alternative indicator that has been shown to be particularly relevant for a variety of socio-economic outcomes including climate risk vulnerability[17]. Keeping the other parameters of $Impact_{mor}^{climate}$ at the values from their previous calibration to the aggregate impact function, we calibrate the steepness parameter, k_{mor}, according to the education-mediated mortality impacts for each discrete value of the independent education variable (MYS or FE). The resulting relationship between steepness and the respective education measure can be seen

in Figure 13b and c. In the baseline scenarios, we set the switch for the impact of education on climate mortality (S_{mor}) equal to 1, meaning that we use the formulation dependent on MYS for the education impacts on climate mortality.

$$Impact_{le}^{climate}(t) = \frac{1}{1 + Impact_{mor}^{climate}(t)} \tag{2.12}$$

$$Impact_{mor}^{climate}(t) = -y_{mor} + \frac{L_{mor}}{1 + e^{-k_{mor}(t) \times (T(t) - x_{0,mor})}} \tag{2.13}$$

$$k_{mor}(t) = \begin{cases} 0, & if\ S_{mor} = 0 \\ f_{mor}^{MYS}\big(MYS(t)\big), & if\ S_{mor} = 1 \\ f_{mor}^{FE}\big(FE(t)\big), & if\ S_{mor} = 2 \end{cases} \tag{2.14}$$

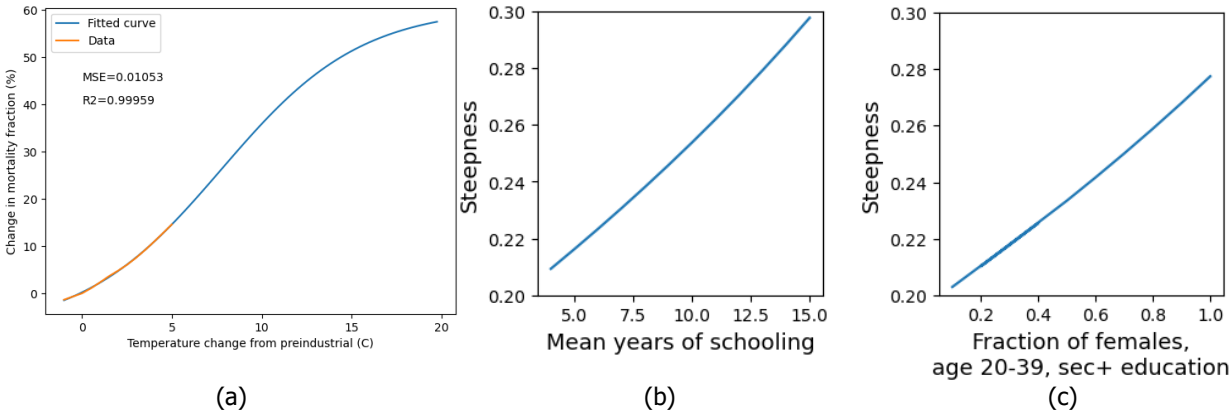

(a) (b) (c)

Figure 13: Calibration results of (a) change in mortality fraction with respect to global mean temperature increase from pre-industrial times, where the data shown in the orange line refer to the empirical estimates[13]; (b) the change in the steepness of the climate mortality function with respect to mean years of schooling; (c) the change in the steepness of the climate mortality function with respect to the share of 20-39 year-old females with minimum secondary education.

Finally, *Life expectancy at birth* (*LE*) is converted to *life expectancy* for each age group and gender (LE_{ij}) with constant coefficients (φ_{ij}) as shown in Equation 2.15. The ratio of life expectancy at any age to life expectancy at birth has been almost constant over time between 1990 and 2020 (Figure 14). Therefore, the coefficients φ_{ij} are estimated as the mean of historical values between 1990 and 2020 (Equation 2.16).

$$LE_{ij}(t) = LE(t) \times \varphi_{ij} \tag{2.15}$$

$$\varphi_{ij} = \frac{\sum_{t=1990}^{t=2019} \varphi_{ij}(t)}{30} \tag{2.16}$$

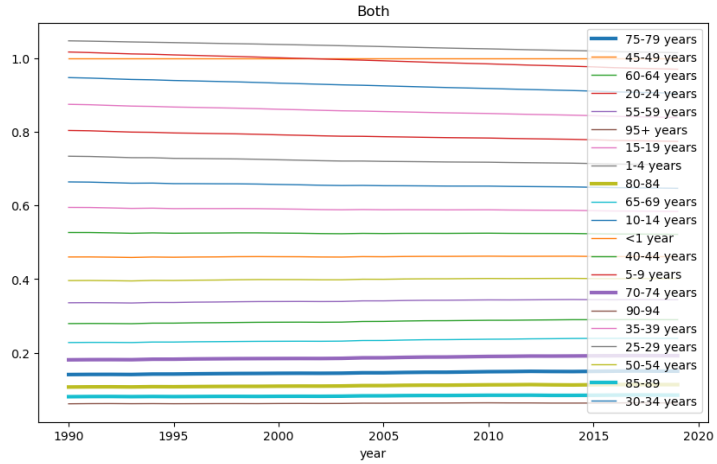

Figure 14: Ratio of life expectancy of each 5-year age group to life expectancy at birth for both genders over time. Data is obtained from the Global Burden of Disease dataset[18].

2.4. Educational attainment and mean years of schooling

The size of different age cohorts feeds into the education module to compute the population of primary, secondary, and tertiary education graduates through the feedback loops among the enrollment rates and graduation rates. The size of the population with each educational attainment level is formulated as another stock chain similar to the population chain shown in Figure 3, to account for the ageing of people who graduate from each level and for transitions between the education levels. Therefore, primary, secondary, and tertiary education graduates are represented by a stock variable for each gender and 5-year age group corresponding to the respective education level.

We make the following assumptions for the correspondence of age groups to education levels:

- Children enroll to primary education when they are 5-9 years old; therefore, the enrollment rate to primary education is a fraction of the population aged 5-9 ($Population_{i,5\text{-}9}$).
- Average duration of primary education is 6 years, as reported by the UNESCO Institute for Statistics for the recent decades. Therefore, children graduate from primary education when they are in the 10-14 or 15-19 age groups.
- A fraction of 10-14 and 15-19 years old primary education graduates enroll into secondary education. Average duration of secondary education is also 6 years, such that people are in the 15-19, 20-24 or 25-29 age groups when they graduate from secondary education.
- Enrollment to tertiary education occurs only in the 15-19, 20-24 and 25-29 age groups, and the average duration of tertiary education is 5 years. Therefore, people join the stock of tertiary education graduates in the age groups 20-24, 25-29 and 30-34.

2.4.1. Primary education

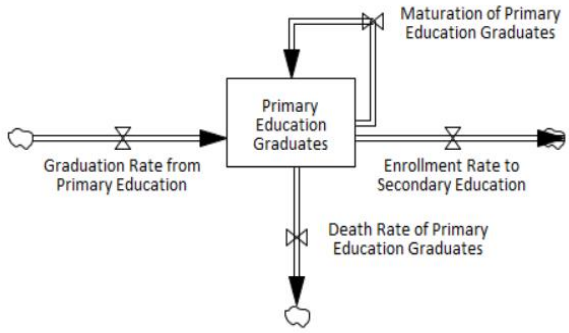

Figure 15: Stock-flow structure of the primary education graduates

The stock-flow structure repeatedly used for all education levels is exemplified in Figure 15, in a compact form of the ageing chain. The net rate of change of the primary education graduates (*PEG$_{ij}$*) for each gender-age group is formulated in Equation 2.17. Maturation ($Maturation_{ij}^{pri}$) and Death ($Death_{ij}^{pri}$) rates of primary education graduates are formulated as fractions of the maturation and death rates for the entire population, where this fraction is the ratio of primary education graduates to the total population, as shown in Equations 2.18 and 2.19.

$$\frac{dPEG_{ij(t)}}{dt} = \begin{cases} 0 \quad ; \quad if\ j\ in\ \{0\text{-}4,5\text{-}9\} \\ Graduation_{ij}^{pri}(t) - Enrollment_{ij}^{sec}(t) - Maturation_{ij}^{pri}(t) - Death_{ij}^{pri}(t) \quad ; \quad if\ j\ in\ \{10\text{-}14,15\text{-}19\} \\ Maturation_{ij-1}^{pri}(t) - Maturation_{ij}^{pri}(t) - Death_{ij}^{pri}(t) \quad ; \quad if\ j > 20\text{-}24 \end{cases} \tag{2.17}$$

$$Maturation_{ij}^{pri}(t) = Maturation_{ij}(t) \times \frac{PEG_{ij}(t)}{Population_{ij}(t)} \tag{2.18}$$

$$Death_{ij}^{pri}(t) = Death_{ij}(t) \times \frac{PEG_{ij}(t)}{Population_{ij}(t)} \tag{2.19}$$

The graduation rate from primary education ($Graduation_{ij}^{pri}$) is equal to enrollment rate to primary education ($Enrollment_{i}^{pri}$), yet after a delay (d_{pri}) equal to the average duration of primary education. *DELAY1* is a function that represents first order exponential delay. Following enrollment within the age group 5-9, we assume that 80% of the children graduate when they are 10-14 years old, and 20% graduate when they are 15-19 years old.

$$Graduation_{ij}^{pri}(t) = \begin{cases} DELAY1\left(Enrollment_{i}^{pri}(t), d_{pri}\right) \times \frac{4}{5} \quad ; \quad if\ j = 10\text{-}14 \\ DELAY1\left(Enrollment_{i}^{pri}(t), d_{pri}\right) \times \frac{1}{5} \quad ; \quad if\ j = 15\text{-}19 \end{cases} \tag{2.20}$$

The enrollment rate is a fraction of the population aged 5-9. The primary education enrollment fraction (*PEF*) for each gender is defined as a reference value (PEF_i^*) multiplied by the impact of GDP ($Impact_{i,pri}^{gdp}$). PEF_i^*corresponds to the maximum possible enrollment fraction. According to the formulation in Equation 2.23 the impact of GDP is assumed to be a logistic (S-shaped) function that saturates at 1 , where the parameters *P$_2$* and *P$_0$* refer to the steepness and inflection point, respectively, and where $GWP\ per\ Capita^*$ is the ratio of gross world product per capita to its value in 2000.

$$Enrollment_{i}^{pri}(t) = Population_{i,5-9}(t) \times PEF_i(t) \tag{2.21}$$

$$PEF_i(t) = PEF_i^* \times Impact_{i,pri}^{gdp}(t) \tag{2.22}$$

$$Impact_{i,pri}^{gdp}(t) = \frac{1}{1 + e^{-P_{2,i} \times (GWP\ per\ Capita^*(t) - P_{1,i})}} \tag{2.23}$$

The formulation of secondary and tertiary education graduates follows Equations 2.17-23, with differences in the age groups explained in the list of assumptions above. Enrollment to secondary (tertiary) education is assumed to be fraction of the primary (secondary) education graduates, implying that the previous education level is a prerequisite for enrollment. The effect of GWP on enrollment for each education level is calibrated to historical data from Wittgenstein Center Human Capital Data Explorer for the period 1950-2020, and the updated SSP2 projections for the rest of the century. Figure 16a shows the calibration results for the f the impact of GDP on primary, secondary and tertiary education enrollment. The effect of GDP on secondary education enrollment is much steeper than the effect on tertiary education, yet the effect on primary education is much flatter, resonating with the historical observations that primary education enrollment is triggered mostly by regulation rather than income . Figure 16b-d show the model-generated dynamic behavior in the reference simulation and the historical data for the three education levels. The difference between model behavior and observed data can be attributed to the limitations of the model structure described above, such as the persistence rates at primary and secondary education persistence of pupils to graduate after enrollment) that are excluded from the model , and our set assumptions about the enrollment ages. It is important to note that Figure 16 visualizes the model output in a business-as-usual (BAU) scenario aligned with SSP2 narrative. The other two baseline scenarios, corresponding to SSP1 and SSP3, used for analyzing the future wellbeing dynamics (Section 5.1) deviate from this BAU scenario and thus imply different model-generated educational attainment dynamics.

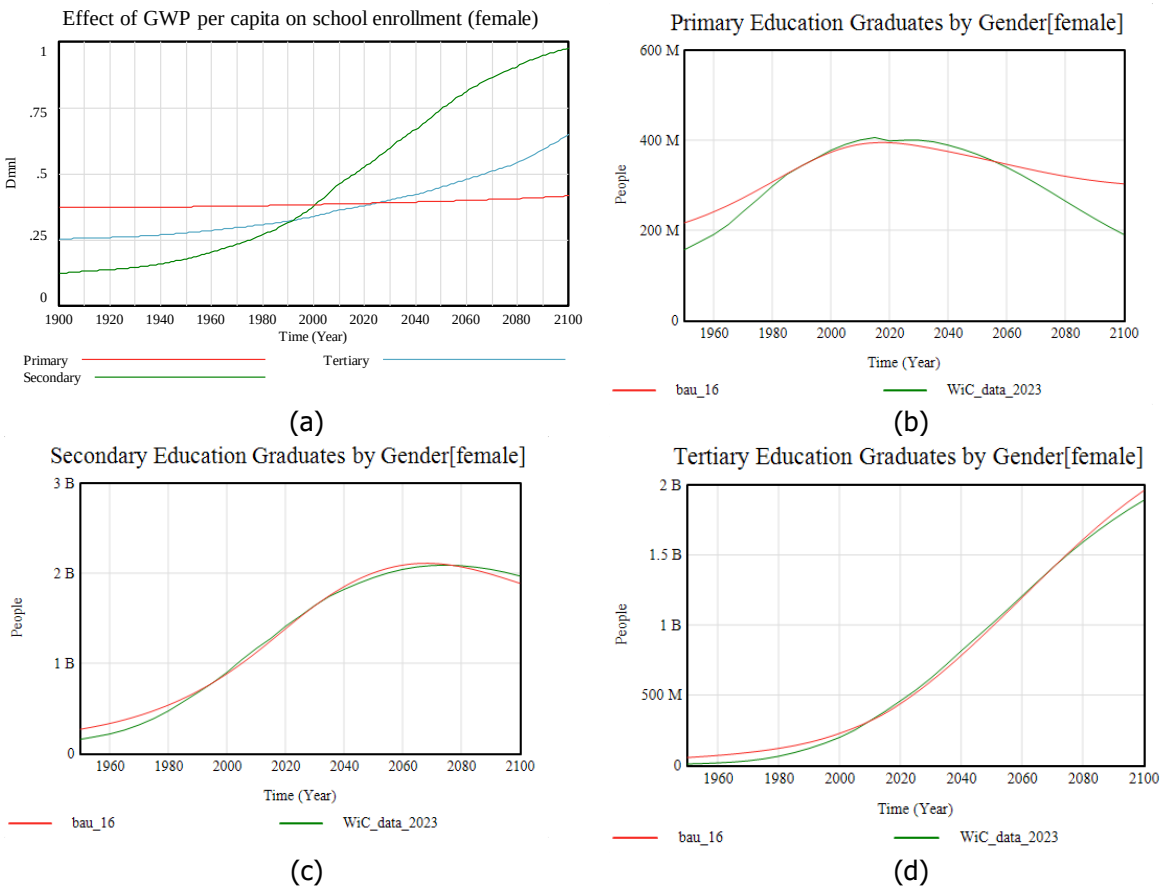

Figure 16: Calibration of the education module for females: (a) Impact of GDP per capita on enrolment to each education level, (b-d) Primary, secondary, and tertiary education graduates over time in the BAU simulation (bau_16) and the historical data obtained from the Wittgenstein Center, including the updated SSP2 projections for the post 2020 period (WiC_data_2023).

2.4.2. Mean years of schooling

Mean years of schooling (MYS) is the indicator used in defining the effect of education on fertility rates and life expectancy. We formulate MYS as the weighted average of the duration of each education level, where the weights are determined by the total number of graduates for the respective education level relative to the population aged 15 and above. Note that this formulation does not include schooling that results in drop-out. Equation 2.24 denotes this formulation, where *SEG* and *TEG* refer to secondary and tertiary education graduates, respectively.

$$MYS(t) = \frac{d_{pri} \times \sum_{j \geq 15} PEG_j(t) \; + \; (d_{pri} + d_{sec}) \times \sum_{j \geq 15} SEG_j(t) \; + \; (d_{pri} + d_{sec} + d_{ter}) \times \sum_{j \geq 15} TEG_j(t)}{\sum_{j \geq 15} Population_j(t)} \qquad (2.24)$$

MYS would be overestimated with the current average durations reported by UN IES, yet there is no data available for the historical average duration of education at each level. Therefore, we assume that the average primary education duration was 2 years in the year 1900 and subsequently increased at an increasing rate to 6 years. Similarly, secondary and tertiary education duration is assumed to start from 1 and 2 years, respectively, in 1900, and subsequently to increase to the current duration of 6 and 5 years, respectively. Figure 17 shows the model behavior resulting from this formulation in comparison to the historical data and SSP2 projections.

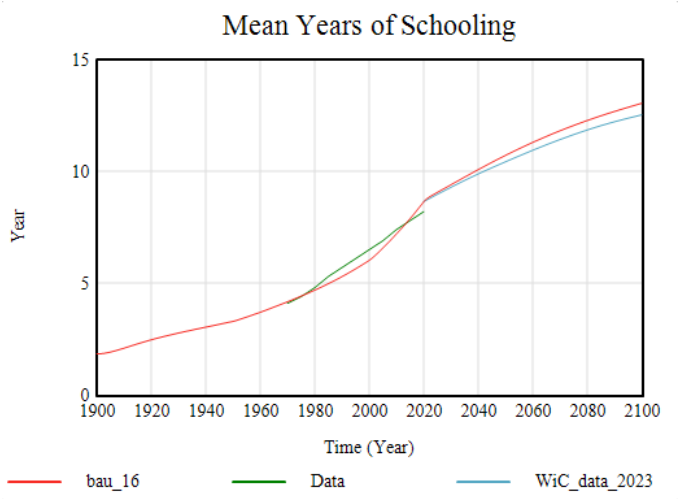

Figure 17: Mean Years of Schooling in the reference simulation results (BAU, red line) and historical data (Data, green line). Data is obtained from the Wittgenstein Centre Human Capital Data Explorer[10] and includes the SSP2 projections updated in 2023 (blue line).

2.5. Labor force

We assume that the size of the skilled labor force is the sum of the total population aged 15-64 with tertiary education, and half of the population aged 15–64 with secondary education (Equation 2.25, j=15-64). The size of the unskilled labor force is determined by the remaining population aged 15–64 (Equation 2.26). The labor force input in the calculation of the economic output is the corresponding labor force multiplied by the labor force participation rates for the respective groups (Equations 2.27 and 2.28).

$$LF_{i,j}^{skilled}(t) = Tertiaty\ education\ graduates_{i,j}(t) + 0.5 \times Secondary\ education\ graduates_{i,j}(t) \qquad (2.25)$$

$$LF_{i,j}^{unskilled}(t) = NonEducated_{i,j}(t) + Primary\ education\ graduates_{i,j}(t) + 0.5 \times Secondary\ education\ graduates_{i,j}(t) \quad (2.26)$$

$$LFinput_{i,j}^{skilled}(t) = \frac{LF_{i,j}^{skilled}(t)}{Initial\ LF_{i,j}^{skilled}} \times LF\ participation\ rate_{i,j}(t) \quad (2.27)$$

$$LFinput_{i,j}^{unskilled}(t) = \frac{LF_{i,j}^{unskilled}(t)}{Initial\ LF_{i,j}^{unskilled}} \times LF\ participation\ rate_{i,j}(t) \quad (2.28)$$

3. Economy

3.1. GDP

Gross world production (GWP) is calculated by total reference economic output (REO), adjusted for the impact of climate change $IF_{\substack{climate \\ on\ GWP}}$ and biodiversity $IF_{\substack{biodiversity \\ on\ GWP}}$ (Equation (3.1)). The total REO is the sum of the REO generated by the skilled and unskilled labor force and determined according to a Cobb-Douglas production function (Equations 3.1-3.4)[19,20], depending on technology and capital allocated to the skilled/unskilled labor force and the size of this labor force input $LFinput_{i,j}^{skilled/unskilled}$. In FeliX, technological progress is assumed to relate to the energy technology and all other technology (Equation 3.5), where the energy technology is endogenously determined by investments in the energy module and all other technology follows an exogenous trend. Capital is determined by capital investments in the energy and all other sectors, which are also captured within the energy module and as an exogenous trend, respectively (Equations 3.6-3.7). The shares of technology and capital, $Ratio\ of\ technology_{skilled}$, $Ratio\ of\ capital_{skilled}$, , attributed to the skilled and unskilled, sectors, respectively, and the capital elasticity of output for the two sectors, $c_{skilled}$, $c_{unskilled}$, respectively, are assumed to be exogenous parameters and determined by the model calibration based on historical data of GWP and GWP per capita from the World Bank[11].

$$GWP(t) = REO(t) \times IF_{\substack{climate \\ on\ GWP}}(t) \times IF_{\substack{biodiversity \\ on\ GWP}}(t) \tag{3.1}$$

$$REO(t) = REO_{skilled}(t) + REO_{unskilled}(t) \tag{3.2}$$

$$REO_{skilled}(t) = REO_{initial} \times Output_{1900} \times Ratio\ of\ technology_{skilled}(t) \times Technology(t) \times \left(Ratio\ of\ capital_{skilled}(t) \times \frac{Capital(t)}{Capital_{inital}}\right)^{c_{skilled}} \times \sum_{i,j=15-64} LFinput_{i,j}^{skilled\ (1-c_{skilled})}(t) \tag{3.3}$$

$$REO_{unskilled}(t) = REO_{initial} \times Output_{1900} \times (1 - Ratio\ of\ technology_{skilled}(t)) \times Technology(t) \times \left((1 - Ratio\ of\ capital_{skilled}(t)) \times \frac{Capital(t)}{Capital_{inital}}\right)^{c_{unskilled}} \times \sum_{i,j=15-64} LFinput_{i,j}^{unskilled\ (1-c_{unskilled})}(t) \tag{3.4}$$

$$Technology(t) = Energy\ Technology(t) + Other\ Technology(t) \tag{3.5}$$

$$\frac{dCapital(t)}{dt} = Capital\ investment(t) \tag{3.6}$$

$$Capital\ investment(t) = Capital\ investment_{energy}(t) + Capital\ investment_{other}(t) \tag{3.7}$$

3.2. Climate impacts

The earlier versions of the FeliX model included climate damages on GDP based on early estimates as used in the DICE model[21]. In the last ten years, the estimation of the aggregate economic impact of climate change has been updated substantially based on new empirical data and methods, resulting in larger damage

estimates. In many economic modelling studies[22-25], climate damage is formulated as a fraction of GDP, with a quadratic function that yields additional damages at an increasing rate for a rising global mean temperature anomaly. In an extensive and widely accepted empirical analysis, Burke et al. (2015)[26] estimate the aggregate climate damage based on micro impacts such as the daily temperature effect on labor productivity per person, agricultural productivity and adaptation efforts across different countries. Burke et al. estimate damage at much larger values compared to the earlier literature, even for relatively modest temperatures. In Figure 18, the black line shows the average damage estimate of Burke et al. when rich and poor countries are assumed to respond identically to the temperature change (pooled response), and the annual GDP is assumed to be affected by temperature changes in a 1 year duration (short-run effect). When the countries are assumed to give a differentiated response and long-run (5 year) effects of temperature change are considered, the damage becomes much higher, reaching the upper end of the gray shaded area in Figure 18, reaching almost 80% of loss at 5°C of warming.

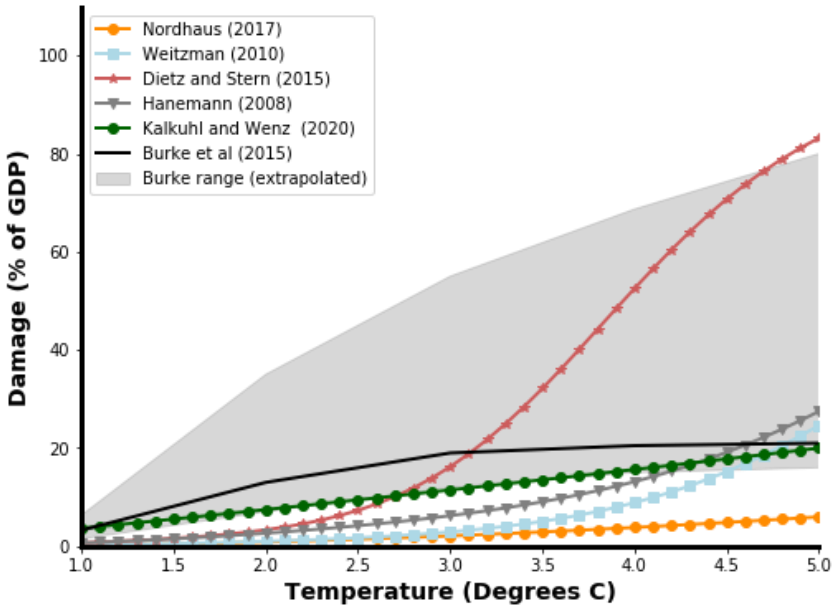

Figure 18: Damage functions and estimates commonly used in the literature

In FeliX, climate damage is formulated as a fraction of global GDP, that is, Gross World Product (GWP). We have an optional structure that enables using the damage functions obtained from the abovementioned studies, or a custom function defined in a flexible logistic form. Equation 3.9 shows this optional formulation, where *Climate Damage Function Switch* (s_{damage}) is the user-defined parameter that enables switching between the options.

$$IF_{\substack{climate \\ on\ GWP}}(t) = 1 - D(t) \tag{3.8}$$

$$D(t) = \begin{cases} 0, if\ s_{damage} = 0 \\ D_N(t), if\ s_{damage} = 1 \\ D_{DS}(t), if\ s_{damage} = 2 \\ D_{B1}(t), if\ s_{damage} = 3 \\ D_{B2}(t), if\ s_{damage} = 4 \\ D_L(t), if\ s_{damage} = 5 \end{cases} \tag{3.9}$$

$D_N(t)$ in Equation 3.10 is the damage function used by Nordhaus (2017)[22], where T is the global mean temperature change from preindustrial times and the parameters α and β are -0.00118 and 0.00278, respectively yielding the percentage damage. Equation 3.11 shows the function used by Dietz and Stern (2015)[23], where the parameters δ_1, $\delta_2, \epsilon_1, \varepsilon_2$ are 12.2, 4, 2 and 7.02, respectively. $D_{B1}(t)\ and\ D_{B2}(t)$ refer to the short-term pooled and long-term differentiated damage estimates of Burke et al. (2015)[26], and they are defined in a lookup form digitalized from the figures in their paper. Table 2 lists those point estimates used in the model.

$$D_N(t) = 1 - \frac{1}{1 + \alpha T(t) + \beta T(t)^2} \tag{3.10}$$

$$D_{DS}(t) = 1 - \frac{1}{1 + \left(\frac{T(t)}{\delta_1}\right)^{\epsilon_1} + \left(\frac{T(t)}{\delta_2}\right)^{\varepsilon_2}} \tag{3.11}$$

Table 2: Damage estimates of Burke et al. (2015) for short-term pooled (D_{B1}) and long-term differentiated (D_{B2}) responses

T (°C)	D_{B1}(%)	D_{B2}(%)
1	1	6.3
2	13	35
3	19	55
4	20.5	68.7
5	21	80

$D_L(t)$ is the logistic function shown in Equation 3.12 that can be used to define custom-shaped damage functions using the three parameters that represent the saturation level (L_{damage}), steepness (k_{damage}) and the inflection point ($x0_{damage}$). The values of these parameters that yield the abovementioned four damage functions can be seen in Table 3.

$$D_L(t) = \frac{L_{damage}}{1 + e^{-k_{damage}(T(t) - x0_{damage})}} \tag{3.12}$$

Table 3: The parameter values of the logistic function calibrated to the four damage functions obtained from the literature

	D_N	D_{DS}	D_{B1}	D_{B2}
L_{damage}	0.073953	0.935478	0.206988	0.75716
k_{damage}	1.09955	1.795846	1.888017	1.43089
$x0_{damage}$	3.89219	3.863367	1.773525	2.2569

3.3. Poverty

The poverty module captures the dynamic relationships between the poverty rate of the global population and relevant drivers from the economy, population, education, as well as the impacts from energy, and land-use modules (Figure 19).

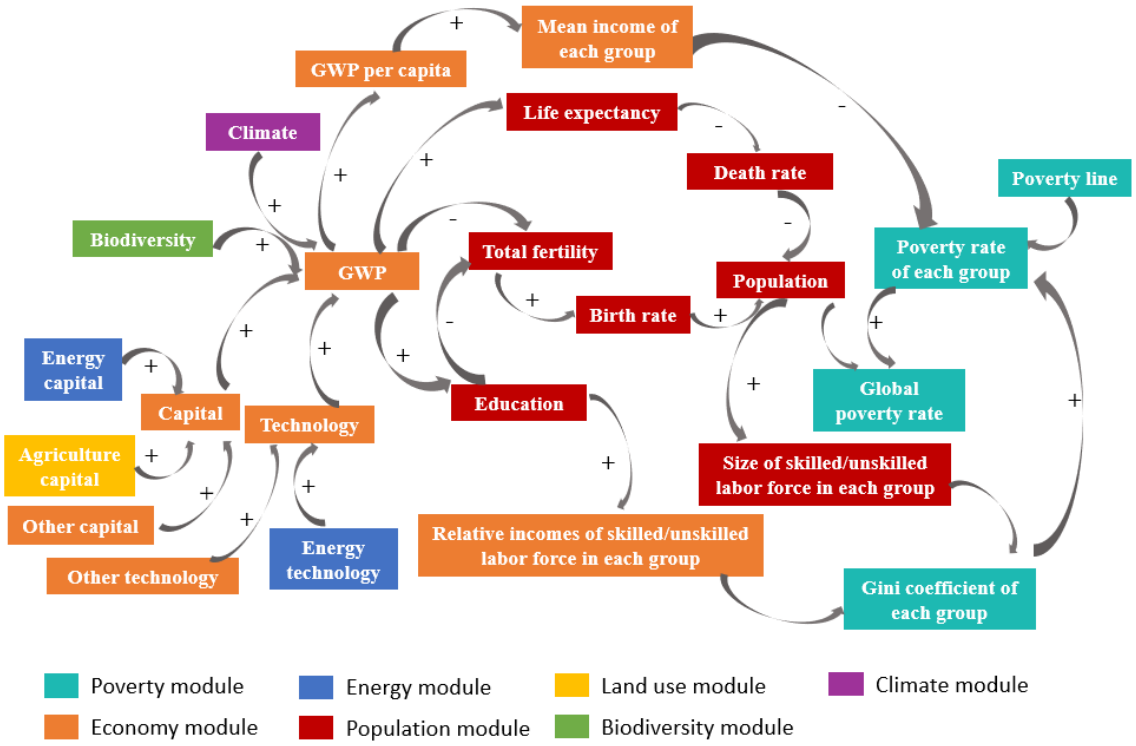

Figure 19: Conceptual relationships between the poverty module and other modules. Each text box indicates a variable, and the background color of the text box indicates the module from which the variable proceeds. Each arrow represents a causal relationship between two variables. The +/- sign on an arrow indicates a positive/negative relationship. The poverty rate of each population group is determined by the poverty line, mean income and Gini coefficient of each group. The Gini coefficient is related to the sizes and relative incomes (incomes share) of skilled and unskilled labor forces.

The global poverty rate *PR* is calculated as the sum of the poverty rates across the different population groups aged over 15 weighted by their corresponding population shares (Equation 3.13).

$$PR(t) = \frac{\sum_{i=male,female} \sum_{j=15-19}^{100+} PR_{i,j}(t) \times Population_{i,j}(t)}{\sum_{i=male,female} \sum_{j=0-4}^{100+} Population_{i,j}(t)} \quad (3.13)$$

The poverty rate $PR_{i,j}$ of each population group is defined as the share of the population living below a specified poverty level *PL*[19,27] (Figure 20). In the calculation of $PR_{i,j}$, income is assumed to follow a log-normal distribution, which has been widely used in the assessment of global and regional inequality and poverty[19,28-30] and has been verified by statistical analyses for various data sets[31-33]. Therefore, $PR_{i,j}$ is formulated as:

$$PR_{i,j}(t)(x \leq PL) = \emptyset\left(\frac{\ln(PL) - \mu_{i,j}(t)}{\sigma_{i,j}(t)}\right) \quad (3.14)$$

where *x* is the income per capita of each group, where *PL* is set to the international extreme poverty line ($2.15 per capita per day in 2017 purchasing power parity), and where μ and σ are the mean and the standard deviation of the normal distribution function of *ln(x)*, respectively.

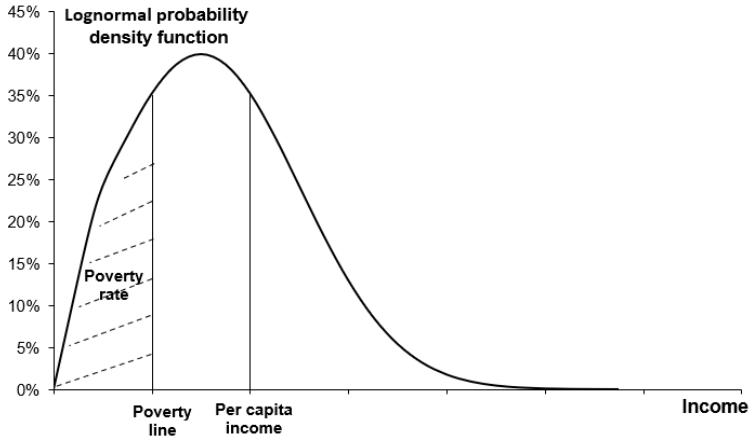

Figure 20: The lognormal probability density function of income. The shaded area is equal to the poverty rate.

The standard normal cumulative distribution function $\emptyset(X)$ is formulated by Equation 3.15, the value of which can be obtained by looking up the standard normal distribution table. The probability density function of income is shown by Equation 3.16 (Figure 20)[34,35]. Let μ and σ denote the mean value and the standard deviation of the normal distribution function $N(\mu,\sigma)$. Then $X = \frac{\ln(PL)-\mu_{i,j}(t)}{\sigma_{i,j}(t)}$ conforms to the standard normal distribution.

$$\emptyset\left(\frac{\ln(x)-\mu_{i,j}(t)}{\sigma_{i,j}(t)}\right) = \int_{-\infty}^{\frac{\ln(x)-\mu_{i,j}(t)}{\sigma_{i,j}(t)}} \frac{1}{\sqrt{2\pi}} e^{-\frac{\left(\ln(x)-\mu_{i,j}(t)\right)^2}{2\sigma_{i,j}^2(t)}} dx \tag{3.15}$$

$$f(x,\mu,\sigma,t) = \frac{1}{\sqrt{2\pi}\sigma_{i,j}(t)} e^{-\frac{\left(\ln(x)-\mu_{i,j}(t)\right)^2}{2\sigma_{i,j}^2(t)}}, \ln(x) \sim N(\mu,\sigma) \tag{3.16}$$

To get the poverty rate $PR_{i,j}$ of each group, given the poverty line, only $\mu_{i,j}$ and $\sigma_{i,j}$ need to be computed. Equations 3.17 and 3.18 formulate the relationship between income per capita, $\mu_{i,j}$, and $\sigma_{i,j}$ [36,37] of each group. $\sigma_{i,j}$ can be expressed as a function of the Gini coefficient, whereas $\mu_{i,j}$ is a function of $\sigma_{i,j}$ and the income per capita of the population[37]. $\emptyset^{-1}(\cdot)$ is the inverse standard normal cumulative distribution function, the value of which can be obtained through the inverse query of the standard normal distribution. To calculate $\mu_{i,j}$ and $\sigma_{i,j}$, we thus need to calculate the Gini coefficient and income per capita.

$$e^{\mu_{i,j}(t)+\frac{\sigma_{i,j}^2(t)}{2}} = Income\ per\ capita_{i,j}(t) \tag{3.17}$$

$$\sigma_{i,j}(t) = \sqrt{2}\emptyset^{-1}\left(\frac{Gini_{i,j}(t)+1}{2}\right) \tag{3.18}$$

The Gini coefficient is a numerical value derived from the Lorenz curve[38] Figure 21as a graphical measure of the income distribution (Figure 21)(3.19). Let *A* denote the area between the perfect equality line and the Lorenz curve, and *B* the area beneath the Lorenz curve (Figure 21). The Gini coefficient for each population group can thus be defined by Equation 3.19(3.19)[37]. Following the International Futures model[19], we divide the labor force of each group into unskilled and skilled. *B* can thus be expressed as the sum of B_1 and B_2,

which represent the areas beneath the Lorenz curve for the unskilled and skilled labor force, respectively (Figure 21).

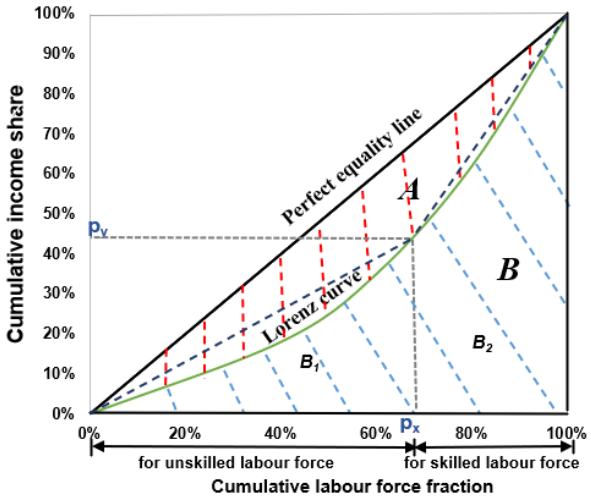

Figure 21: Income distribution measured by Lorenz curve. The cumulative labor force fraction at a point on the x-axis is defined as the size of cumulative labor force at this point divided by the size of the total labor force. The x-value of px and a y-value of py mean that the unskilled labor force (the bottom px of the labor force) controls the proportion py of the total income. The Gini coefficient is a numerical value derived from the Lorenz curve to measure income distribution, which is defined as *A / (A+B)*. Here, *A* and *B* represent the sizes of the red and blue striped areas . *B* is the sum of B_1 and B_2. The sum of *A* and *B* is 0.5. The perfect equality line corresponds to a Gini coefficient of 0, indicating that every person has the same income.

By using a triangle and a trapezoid to approximate the areas of B_1 and B_2[19], the Gini coefficient can be reformulated by Equation 3.20. $Relative\ income_{i,j}^{Total}$, $Relative\ income_{i,j}^{unskilled}$ and $Relative\ income_{i,j}^{skilled}$ denote the relative income share of the total, unskilled, and skilled labor force of the corresponding population group, respectively. $Population_{i,j}^{unskilled}$ and $Population_{i,j}^{skilled}$ denote the population size of the total, unskilled, and skilled labor force of the corresponding population group, respectively.

$$Gini_{i,j}(t) = \frac{A_{i,j}(t)}{A_{i,j}(t)+B_{i,j}(t)} = \frac{0.5-B_{i,j}(t)}{0.5} = 1 - 2B_{i,j}(t) \tag{3.19}$$

$$Gini_{i,j}(t) = 1 - \frac{1}{Relative\ income_{i,j}^{Total} \times Population_{i,j}(t)} \times \begin{pmatrix} Population_{i,j}^{unskilled}(t) Relative\ income_{i,j}^{unskilled} \\ +Population_{i,j}^{skilled}(t)\left(2Relative\ income_{i,j}^{unskilled} + Relative\ income_{i,j}^{skilled}\right) \end{pmatrix} \tag{3.20}$$

The value of $Relative\ income_{i,j}^{Total}$ is assumed to be 100. The values of $Relative\ income_{i,j}^{unskilled}$ and $Relative\ income_{i,j}^{skilled}$ are based on relative earnings data for OECD countries[39] (Equations 3.21 and 3.22). The value 65 approximates the average relative earnings share of the skilled population in OECD countries. The $Adjustment\ parameter\ for\ relative\ incomes\ of\ skilled_{i,j}$ for each group adjust the relative incomes of skilled labor force in line with the model calibration.

$$Relative\ income_{i,j}^{skilled} = 65 \times Adjustment\ parameter\ for\ relative\ incomes\ of\ skilled_{i,j} \tag{3.21}$$

$$Relative\ income_{i,j}^{unskilled} = Relative\ income_{i,j}^{Total} - Relative\ income_{i,j}^{skilled} \quad (3.22)$$

$Income\ per\ capita_{i,j}$ is formulated by Equation 3.23, where $Real\ earnings\ parameter_{i,j}$ is determined by model calibration.

$$Income\ per\ capita_{i,j}(t) = GWP\ per\ capita(t) \times Real\ earnings\ parameter_{i,j} \quad (3.23)$$

In the model calibration, values of $Adjustment\ parameter\ for\ relative\ incomes\ of\ skilled_{i,j}$ and $Real\ earnings\ parameter_{i,j}$ are determined based on three assumptions: (1) the relationship between income and age tends to exhibit an inverted-U-shape pattern. Income rises with age and then drops slightly as individuals enter retirement[40,41]. (2) Males have more income than females in the same age group[42,43]. (3) The relative income share of the skilled population in each group is larger than that of unskilled population. In addition, due to the limited availability of relevant historical data and in order to make the calibration process more reliable, the population age groups are divided into three wider age groups: childhood (0-14 years old), working age (15-64) and old age (65+). Parameters are then distinguished only across these three age groups.

The model calibration results for global poverty rates are shown in Figure 22.

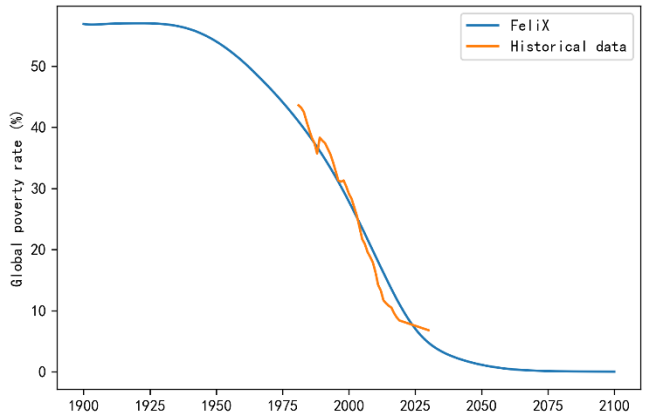

Figure 22: Business-as-usual simulation results for global poverty rates. Source of the historical data: https://data.worldbank.org/indicator/SI.POV.DDAY

4. Wellbeing

We operationalize wellbeing mostly through the novel comprehensive wellbeing indicator YoGL (Years of Good Life), a measure developed by Lutz, et al. [44] which aims at estimating the remaining years of life an individual can expect to live in a "good" state. By considering the changing characteristics of human populations that reflect the overall wellbeing of society, YoGL is specifically designed to assess the sustainability of long-term development trajectories [45].

YoGL is built on the fundamental assumption that for individuals to experience any quality of life, they must first be alive. However, recognizing that mere survival alone is insufficient to capture wellbeing, YoGL is contingent upon meeting minimum standards of both objectively observable conditions (capable longevity) and subjective life satisfaction. Drawing on earlier works by Sen[46], the objective conditions measuring "capable longevity" are further divided into three dimensions: being out of poverty, being cognitively enabled, and being physically healthy. To be considered as "good" years in the YoGL calculation, individuals must surpass critical thresholds in all three objective dimensions and report also a minimum level of overall life satisfaction.

To calculate YoGL, we apply the well-established Sullivan method[47]. It combines data from a regular life table with cross-sectional data on a specific phenomenon of interest, allowing for the quantification of proportions of the population in different states. In the case of YoGL, the state space includes different levels of subjective satisfaction with life, as well as the objectively assessed states of poverty, cognition, and health. The proportions of people in different states are calculated at different ages before they are used as weights for the age-specific life table person years lived, from which life expectancies in different states can be obtained using conventional life table techniques. The formula for calculating YoGL at age x is depicted in Equation 4.1:

$$YoGL_x(t) = \frac{1}{l_x(t)} \sum_{j=x}^{A} \pi_j(t)\, L_j(t) \tag{4.1}$$

$$\pi_{ij}(t) = p_{ij}(t)\, h_{ij}(t)\, e_{ij}(t) \tag{4.2}$$

where l_x stands for number of survivors at age x (beginning of interval j), L_j stands for the person-years lived in the age interval j and π_j stands for the prevalence of the state of interest in the age interval j, i.e., age-specific proportions of the population that are not living in poverty, are (at least) in basic physical and cognitive health, and report positive life satisfaction. Finally, A denotes the last (open) age group in the life table (i.e., 100+).

While π_j should be ideally derived from objectively assessed individual characteristics as measured in representative cross-sectional surveys[44], such an approach is not possible to implement in a global macro model such as FeliX. Therefore, the different dimensions of YoGL are estimated as endogenous variables as will be explained further in the following sub-sections. π_j is then calculated as the product of age and gender specific proportions of people out of poverty (p_{ij}), people meeting or exceeding basic health (h_{ij}), and people meeting or exceeding basic cognitive functioning (e_{ij}) as Equation 4.2 shows. Given the lack of data on subjective life satisfaction on the global level, we exclude it from the formulation of the dynamic prevalence rates.

4.1. Being out of poverty

The age- and gender-specific proportion of people out of poverty *($p_{i,j}$)* is directly derived from the poverty rate *$PR_{i,j}$* (as detailed in Section 3.3), following Equation 4.3:

$$p_{ij}(t) = 1 - PR_{ij}(t) \tag{4.3}$$

4.2. Basic physical health

The proportion of people with basic physical health *(h)* is estimated using the ratio of health-adjusted life expectancy *(HALE*) to life expectancy *(LE)*, for each gender *i* and age group *j*, as shown in Equation 4.4.

$$h_{ij}(t) = \frac{HALE_{ij}(t)}{LE_{ij}(t)} \tag{4.4}$$

LE_{ij} is derived from *life expectancy at birth (LE)* as described in Section 2.3. *$HALE_{ij}$* is derived from *healthy life expectancy at birth (HALE$_i$)* with coefficients (ρ_j) estimated from historical data (Equation 4.5). The ratio of *HALE* at any age to *HALE at birth* has been almost constant over time, as shown by historical data obtained from the Global Burden of Disease (GBD) data for the years 1990-2020[18] and depicted in Figure 23. Therefore, the age coefficients of *HALE* are assumed to remain constant in the future, too, and are set equal to the mean of the historical values as shown in Equation 4.6.

$$HALE_{ij}(t) = HALE_i(t) \times \rho_j \tag{4.5}$$

$$\rho_j = \frac{\sum_{t=1990}^{t=2019} \rho_j(t)}{30} \tag{4.6}$$

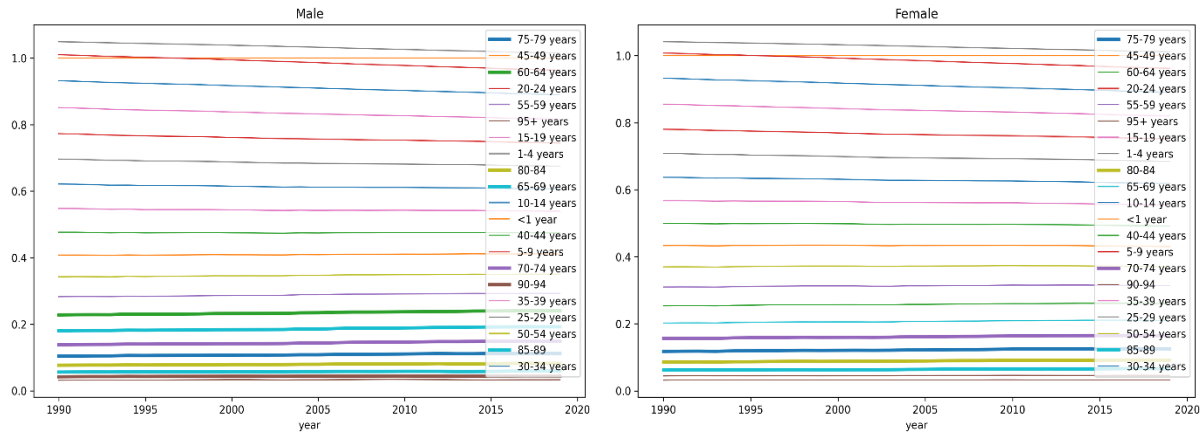

(a) (b)

Figure 23: Ratio of Healthy Life Expectancy to Healthy Life Expectancy at Birth for each 5-year age group and over time for males (a) and females (b)

HALE at birth is formulated as a function of *GDP per capita* and *daily food supply per capita*, especially from sugar and oil crops. This choice was motivated by the recent findings of Aangelo et al. (2022)[48], who analyzed the drivers of *HALE* based on panel data from 30 European countries using machine learning algorithms

designed to infer causality (causal forests). Their findings show that the most important factors affecting HALE are gross national income (GNI) and body mass index (BMI), followed by educational expenditure. This strong relationship between HALE, GDP and BMI can be found in global data too, as demonstrated in Figure 24. In FeliX, we take the GWP per capita as a proxy for GNI, and we approximate BMI by the caloric supply per person. BMI has increased over time depending on food supply, as Figure 25 shows. If BMI continues to increase as a result of food supply, the HALE-food relationship would be reversed, though, due to adverse health effects observed in the overweight population. We derive this non-linear relationship between HALE and food supply from the panel data across 204 countries over years 1990-2019, using *locally estimated scatter plot smoothing*, as demonstrated in Figure 26.

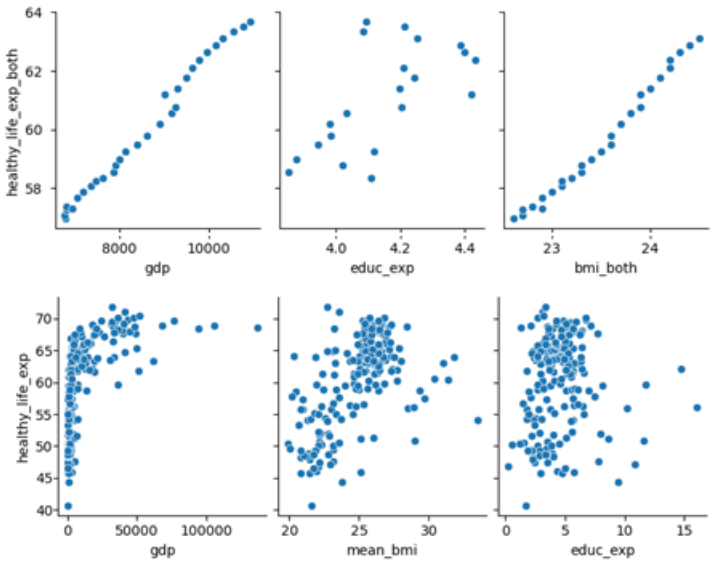

Figure 24: Relationship between average healthy life expectancy at birth (healthy_life_exp) and GDP per capita (gdp), average body mass index (bmi) and educational expenditure as a percentage of GDP (educ_exp). The top row shows the relationships over time, where each data point refers to the global average value in a year between 1990 and 2019. The bottom row shows the relationships across countries, where each data point refers to the values per country averaged over time. The data for healthy life expectancy and BMI is obtained from the Global Burden of Disease dataset. The GDP and educational expenditure data is obtained from the World Bank statistics.

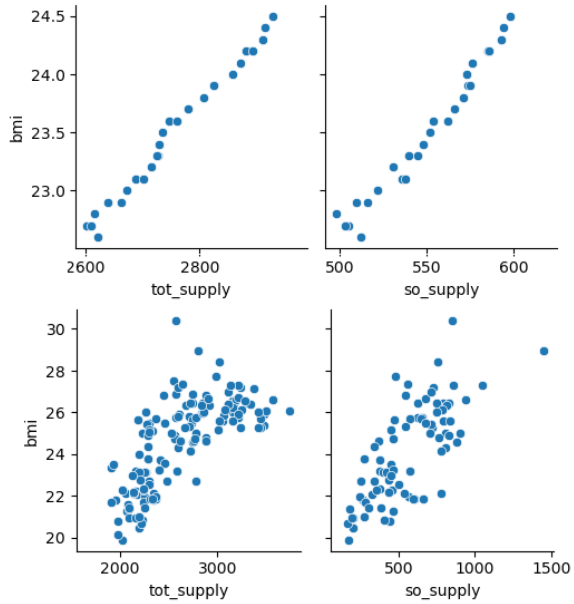

Figure 25: Relationship between body mass index (bmi) and total food supply (tot_supply) and food supply from sugar and oil crops (so_supply) as calories per person per day. The top row shows the relationships over time, where each data point refers to the global average value in a year between 1990 and 2019. The bottom row shows the relationships across countries, where each data point refers to the values per country averaged over time. The data for BMI is obtained from the Global Burden of Disease dataset. The food supply data is from the FAO food balance sheets.

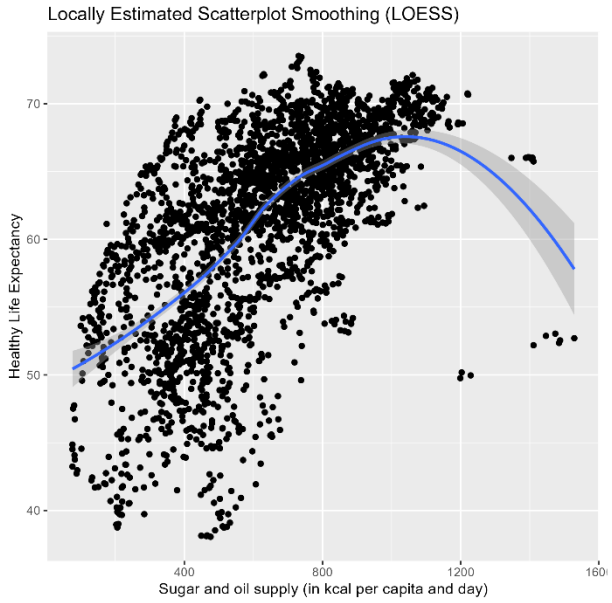

Figure 26: Inverted U-shaped relationship between healthy life expectancy and sugar and oil supply

Therefore, we formulated HALE at birth (*HALE*$_i$) as in Equation 4.7, where the global average HALE for males and females in year 2000 is the reference value, and the impact of food supply and GDP per capita are multipliers over this reference value. The impact of food supply on HALE is formulated as a lookup function (*f*), replicating the approximation in Figure 26, yet normalized on both the x and y axes according to the actual value in year 2000 (Equation 4.8). Considering the logarithmic pattern of relationship observed in Figure 24 between HALE and GDP per capita, we use the exponential function form denoted in Equation 4.9 to define the impact of GDP on HALE. The parameters *a* and *b* are calibrated according to the historical values

of HALE at birth for both males and females in period 1990-2019, after setting the impact of food as defined in Equation 4.8. The resulting function form for the effect of GDP is shown in Figure 27. It is important to note that HALE-GDP relationship is calibrated in an earlier version of the model where the GDP outcome was different, and it will be adjusted in the upcoming revision.

$$HALE_i(t) = HALE_i^{2000} \times Impact_{hale}^{gdp}(t) \times Impact_{hale}^{food}(t) \tag{4.7}$$

$$Impact_{hale}^{food}(t) = f\left(\frac{Food_{oil\&sugar}(t)}{Food_{oil\&sugar}(2000)}\right) \tag{4.8}$$

$$Impact_{hale}^{gdp}(t) = a \times \left(GWP\ per\ Capita^*(t)\right)^b \tag{4.9}$$

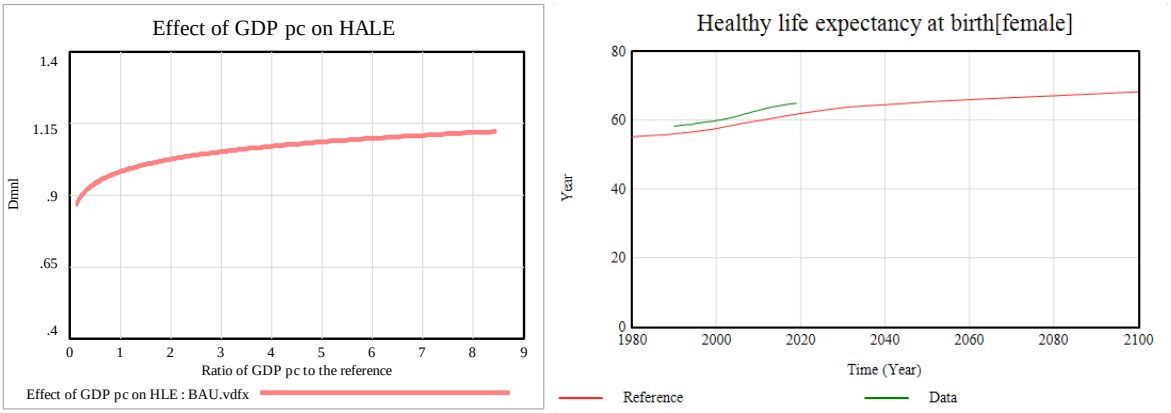

(a) (b)

Figure 27: (a) The impact of GDP on healthy life expectancy and (b) the simulation results for healthy life expectancy at birth of females (green) compared to the historical values (pink) obtained from GBD dataset.

4.3. Being cognitively enabled

In the original definition of YoGL, Lutz et al. use the results of well-established numeracy and memory tests recorded in a multi-national survey. In this global dynamic modelling setting, we use the fraction of population with minimum primary education as a proxy for the cognition component of YoGL. Therefore, the prevalence of cognition component of YoGL is formulated as the sum of primary, secondary and tertiary education graduates (See section 2.4), divided by the population for each age and gender, as denoted in Equation 4.10.

$$e_{ij}(t) = \frac{PEG_{ij}(t) + SEG_{ij}(t) + TEG_{ij}(t)}{Population_{ij}(t)} \tag{4.10}$$

5. Scenario analysis for global wellbeing

5.1. Definition and calibration of the three baseline scenarios

We explore the global well-being dynamics in three baseline scenarios that characterize a neutral business-as-usual (reference), sustainable (optimistic), and unsustainable (pessimistic) world. These three baseline scenarios are aligned with the Shared Socioeconomic Pathways (SSPs)[49] energy, land use, food, and climate policy, following the earlier calibration of the FeliX model to these narratives as described in Moallemi et al.(2022)[7]. Specifically, the reference, optimistic, and pessimistic scenarios follow the SSP2, SSP1, and SSP3 trajectories, respectively. In addition, the radiative forcing of non-CO_2 gases, which are not endogenously modeled in FeliX, is assumed to follow RCP 4.5, RCP 2.6 and RCP 6 in the reference, optimistic, and pessimistic scenario, respectively.

Population and GWP growth also follow the corresponding SSP narratives, taking additional account of climate impacts, which are not considered in the original SSP projections. These climate impacts on mortality and GWP are formulated as described in Sections 2.33.2 and 3.2, respectively, with the eventual impact depending on the temperature projection created by each narrative. To calibrate the demographic variables to the SSPs, we use the population projections updated in 2023 as provided by Wittgenstein Center for Demography and Global Human Capital. For all other variables, we use the SSP baseline projections produced by the integrated assessment modelling community and published in the SSP scenario database[50]. Appendix I lists parameter values of the FeliX model calibrated to each narrative.

Figure 28 shows the dynamic trajectory of global population in the three baseline scenarios and the corresponding SSPs. The *Reference* scenario results in higher population values than SSP2, so does the *Optimistic* scenario but only marginally between 2030 and 2060. This is attributed to fertility rates being higher than their SSP projection due to lower economic growth in the presence of climate damages and due to lower education embedded in the scenario narrative. Still, this means that the direct impact of climate on mortality is not stronger than the economic impact in these two scenarios. In the *Pessimistic* scenario, FeliX projections are lower than SSP3, due to the strong direct climate impact on mortality, and indirect effects through much lower economic growth. Similarly, Figure 29 shows the educational attainment differences between the baseline scenarios and the SSP2 projections, specifically for the global tertiary education graduates. In all three scenarios, FeliX projections are lower than the SSP ones, due to lower economic growth (Figure 30) and the sensitivity of tertiary education enrolment to GWP per capita (Figure 16a).

The three baseline scenarios deviate significantly from their corresponding SSPs in terms of projections of global economic output (GWP) as shown in Figure 30 due to the strong climate damage assumption in the former (Section 3.2). Figure 31 shows the GWP projections in the three baseline scenarios without climate damages, where the difference from the SSPs is smaller, with remaining differences being attributed to the endogenous calculation of economic output in FeliX with different factors. The temperature projections in the three scenarios underlying the economic impacts of climate change are shown in Figure 32.

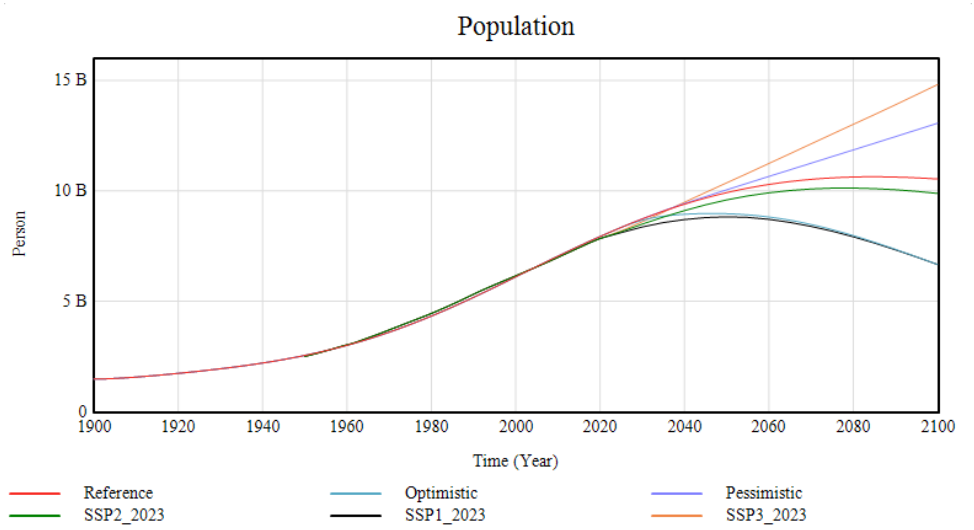

Figure 28: Global population over time in the three baseline scenarios generated by FeliX and in the corresponding SSP projections

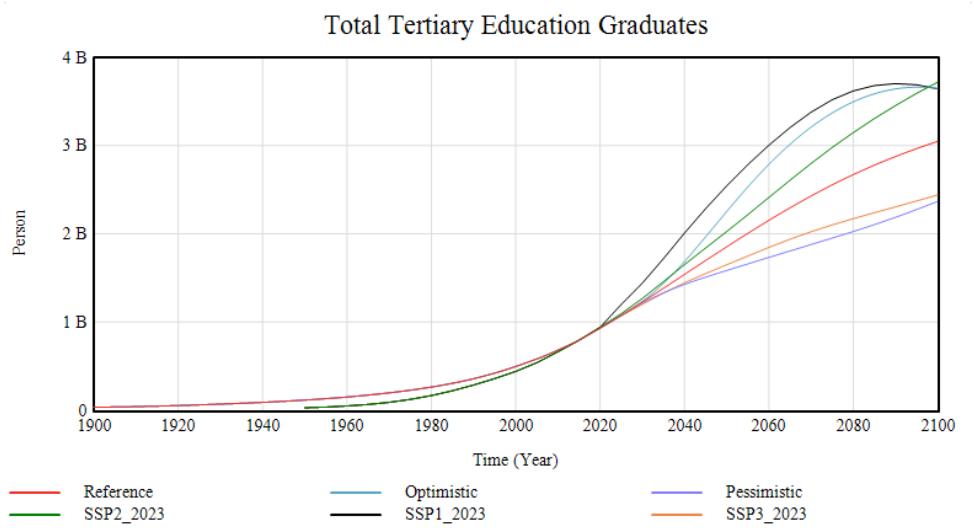

Figure 29: Global tertiary education graduates in the three baseline scenarios generated by FeliX and in the corresponding SSP projections

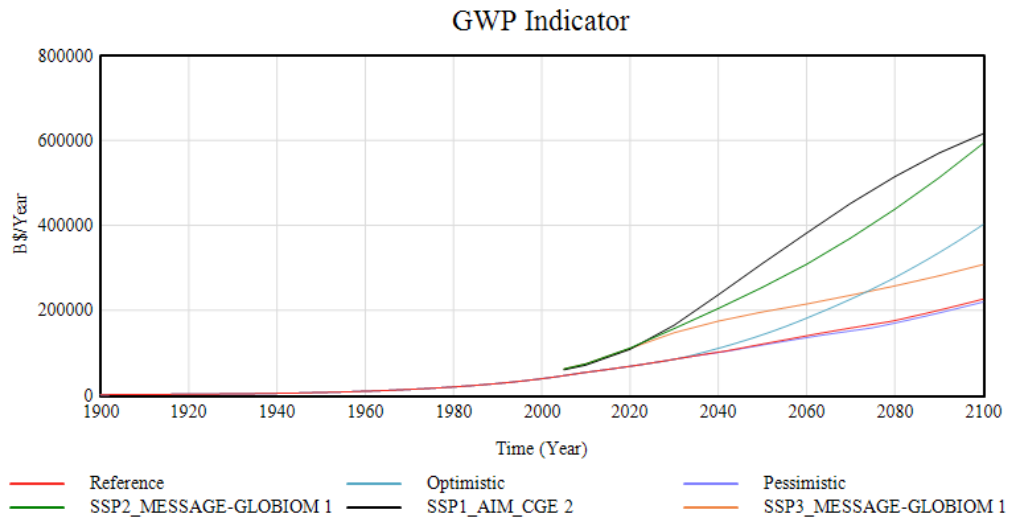

Figure 30: Global GDP (gross world product) in the three baseline scenarios generated by FeliX and in the corresponding SSP projections

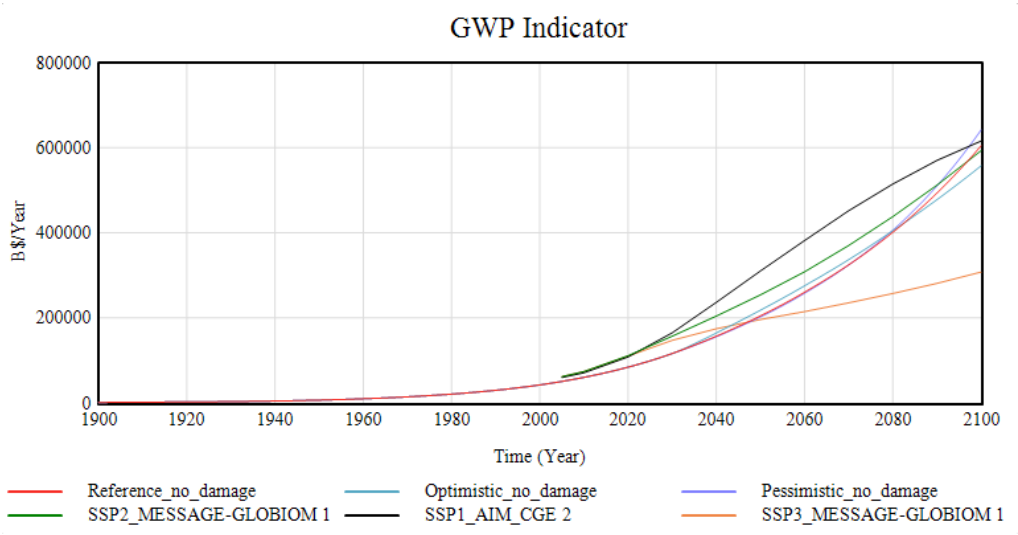

Figure 31: Global GDP (gross world product) in the three baseline scenarios generated by FeliX without climate damages taken into account and in the corresponding SSP projections

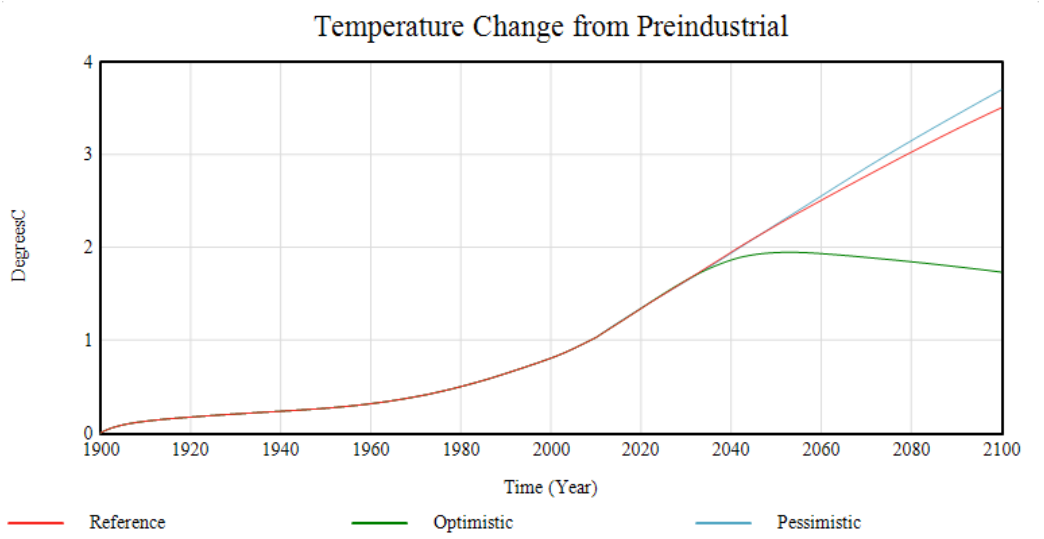

Figure 32: Global mean temperature change from preindustrial times in the three baseline scenarios generated by FeliX

Figure 33-Figure 38 show the comparison of the FeliX projections in the *Reference* scenario to SSP2 projections of various integrated assessment models used in the IPCC assessments. FeliX projects *Total Radiative Forcing* within the range of projections created by other models, except the last two decades of the century, where the FeliX projection declines (Figure 33). This can be attributed to the decline in the CO_2 emissions in the FeliX output in those decades (Figure 34), which is otherwise around 5 Gt/yr higher than the SSP2 projections. Such higher emission projections in the FeliX compared to the other models is due to the differences in the agriculture and land use emissions, amongst other factors. As Figure 35 and Figure 36 show, FeliX projections for the agricultural production from non-energy crops fall within the range of projections by other models, yet the livestock production is on the higher end of that range in the FeliX model, similar to the projections by the REMIND-MAgPIE model. Considering the coal and wind energy production as the two indicators from the energy sector, FeliX projections similarly fall within the range of projections by other models (Figure 37 and Figure 38), with coal production already showing a decline in SSP2 towards the end of the century as in the WITCH-GLOBIOM model.

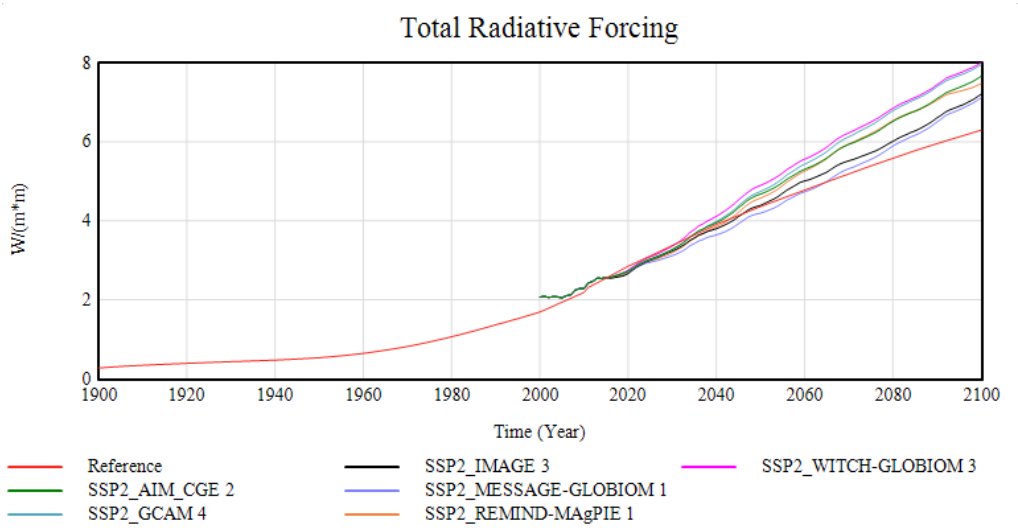

Figure 33:Total radiative forcing in the Reference scenario generated by FeliX and in the SSP2 projections created by six other integrated assessment models

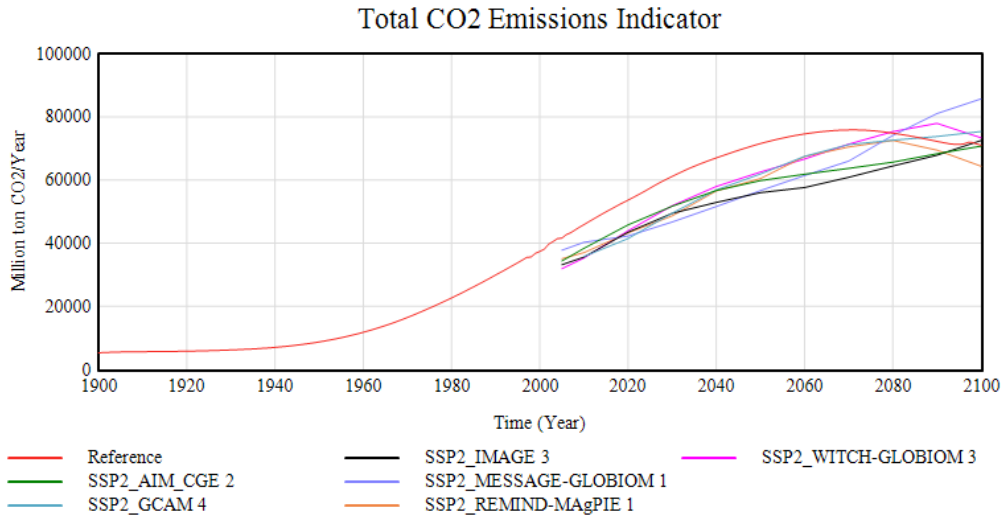

Figure 34: Total global CO_2 emissions in the Reference scenario generated by FeliX and in the SSP2 projections created by six other integrated assessment models

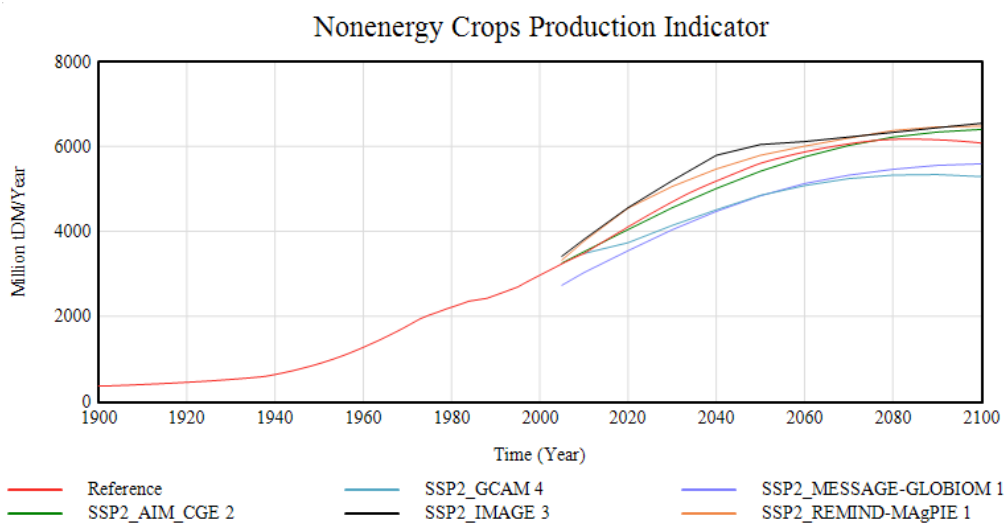

Figure 35: Total agricultural crop production from non-energy crops in the Reference scenario generated by FeliX and in the SSP2 projections created by six other integrated assessment models

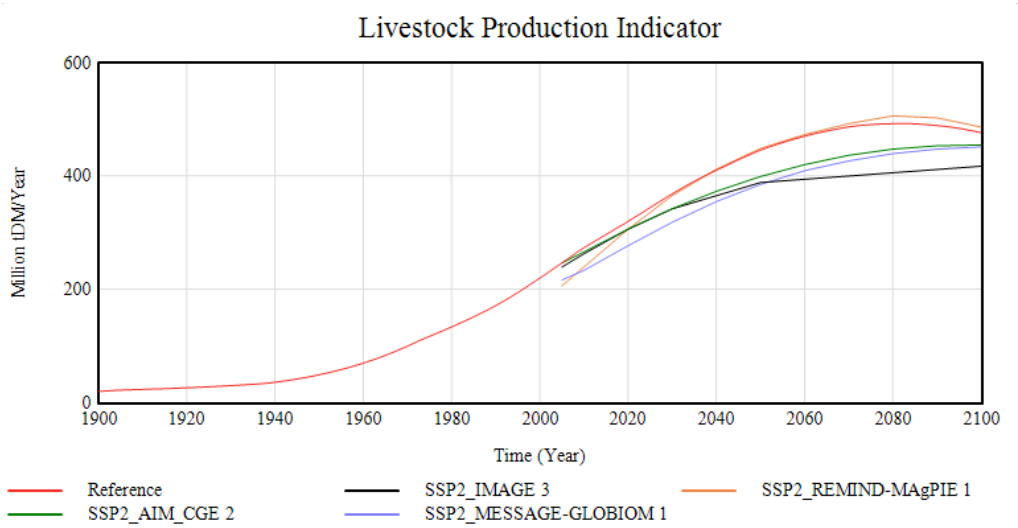

Figure 36: Total agricultural production from livestock in the Reference scenario generated by FeliX and in the SSP2 projections created by six other integrated assessment models

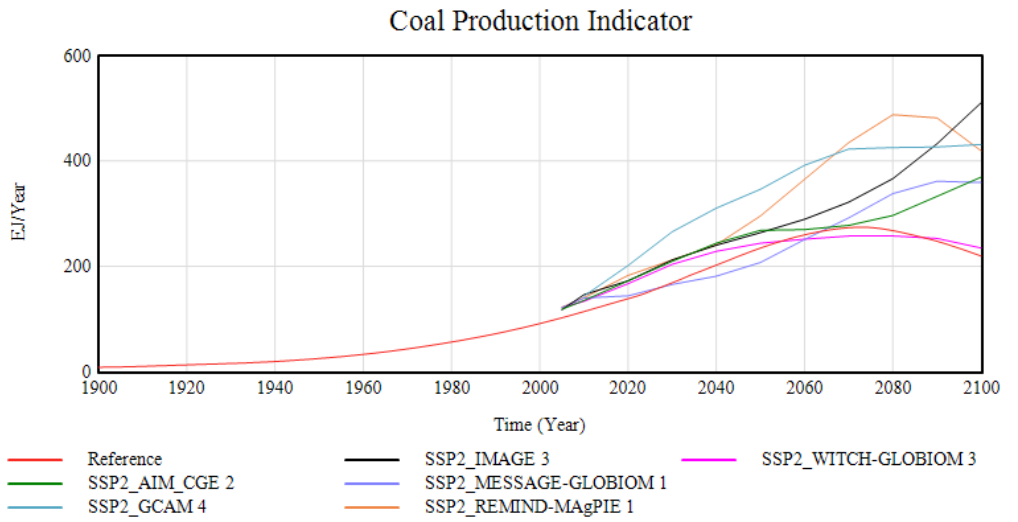

Figure 37: Global primary energy production from coal in the Reference scenario generated by FeliX and in the SSP2 projections created by six other integrated assessment models

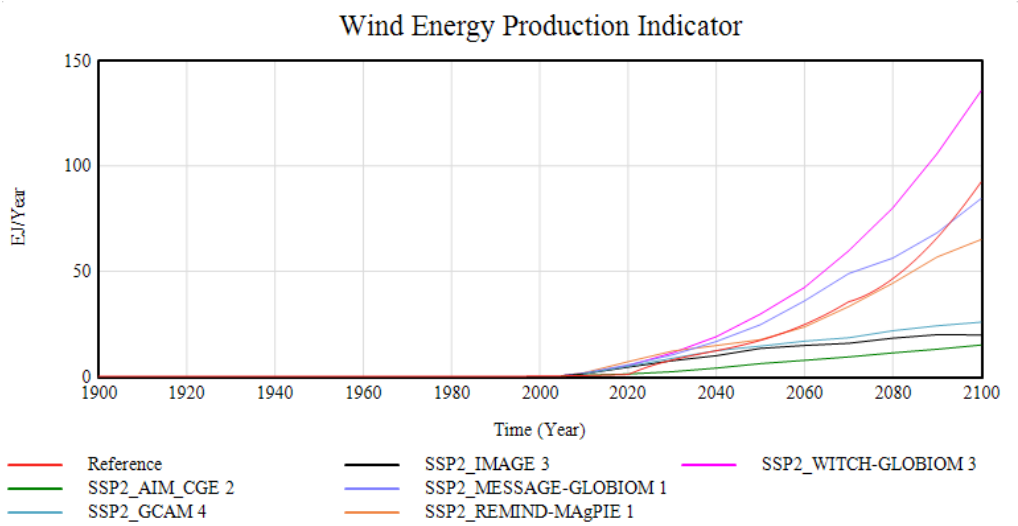

Figure 38: Global primary energy production from wind in the Reference scenario generated by FeliX and in the SSP2 projections created by six other integrated assessment models

5.2. Future dynamics of key indicators in the three baseline scenarios

5.2.1. Education

Economic growth is accompanied by an educational expansion, as depicted by the global total number of tertiary graduates and mean years of schooling (Figure 39). Here, the optimistic scenario features a higher growth of tertiary graduations, which reaches 3.65 billion people by 2100 and can be traced to an earlier and stronger shift in the educational distribution from primary towards tertiary education. In the pessimistic scenario though, educational expansion is halted, as indicated by a much lower increase in population fraction with minimum secondary education compared to the business-as-usual and optimistic scenario (Table 4). Corresponding to these educational attainment levels, global mean years of schooling reaches up to 14.2 years in the optimistic scenario, whereas it remains at 10.3 years in the pessimistic scenario.

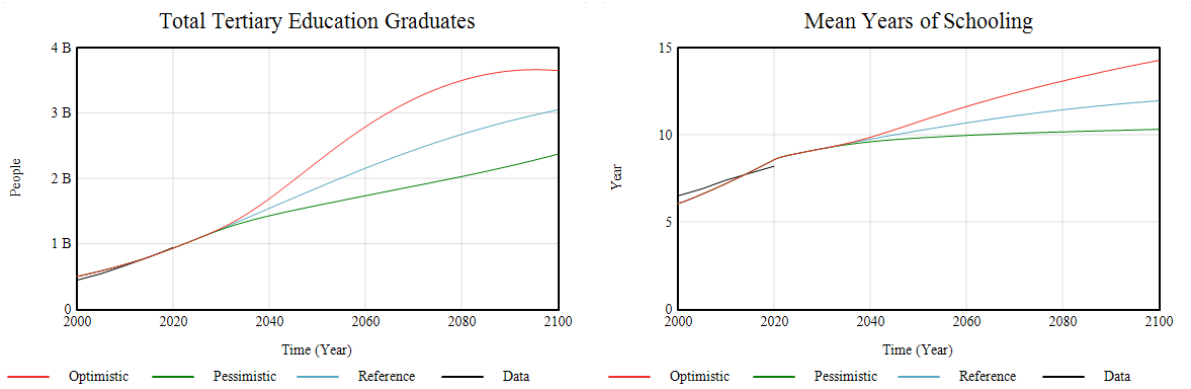

(a) (b)

Figure 39: Projections of global total tertiary education graduates (a) and mean years of schooling (b) in the three baseline scenarios. Historical data (black line) is obtained from Wittgenstein Center for Data Explorer.

Table 4: Summary of model projections for educational attainment in the three baseline scenarios

	Fraction of population with minimum secondary education			Fraction of female population with minimum secondary education		
	2020 (data)	2050	2100	2020 (data)	2050	2100
Optimistic		66%	90%		65%	91%
Reference	48.8%	60%	72%	47.9%	58%	70%
Pessimistic		54%	57%		53%	56%

5.2.2. Poverty

Global poverty, measured by the fraction of global population who live below the $2.15 poverty line, is curbed in all scenarios and close to being eradicated by the year 2100 (Figure 40). This projection of DEMOFelix in the three baseline scenarios resonates with the reported poverty rates (8.5% in 2019 as published by the World Bank) and with similar projections, for instance by the International Futures model used by the United Nations Development Program, that report a rapidly declining trend in the poverty rate in the baseline scenarios[51,52] (Figure 41). Stronger GWP growth in the optimistic scenario allows for a somewhat earlier poverty reduction. Despite this promising global trend, poverty rate remains relatively high in population sub-

groups. For instance, the poverty rate among young females is still 7% in 2040 in the pessimistic scenario, as opposed to the 4% global average poverty rate.

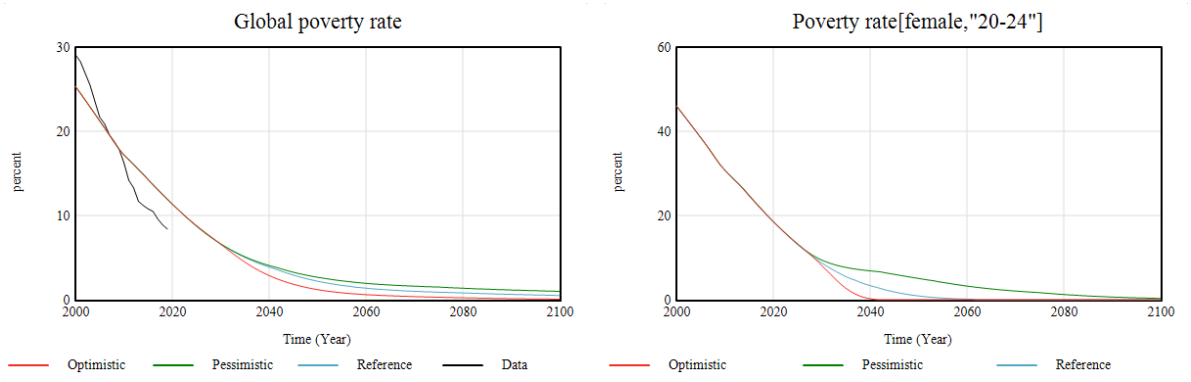

(a) (b)

Figure 40: Projections of global poverty rate (a) and the poverty rate among 20-24 year-old females (b) in the three baseline scenarios. Historical data (black line) for the global poverty rate is obtained from the World Bank statistics.

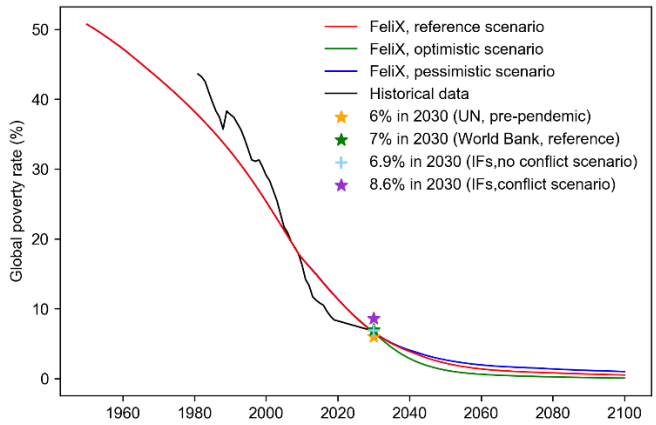

Figure 41: Projections comparison of global poverty rates. UN projected 6% poverty rate in 2030 under a pre-pandemic scenario without considering the pandemic impacts. IFs scenarios are from Burgess, et al. [51].

Appendix I: Parameterization of the baseline scenarios

Parameter	Reference	Optimistic	Pessimistic
Birth Gender Fraction Variation	0.515	0.508	0.511
Normal Fertility Variation	2.630	1.689	3.101
Life Expectancy Variation	65.680	66.668	58.512
Secondary education enrollment Variation[male,"10-14"]	1.000	1.000	1.000
Secondary education enrollment Variation[female,"10-14"]	0.900	1.000	1.000
Secondary education enrollment Variation[male,"15-19"]	0.850	1.000	0.438
Secondary education enrollment Variation[female,"15-19"]	0.850	1.000	0.400
Tertiary education enrollment Variation[male]	0.390	0.690	0.392
Tertiary education enrollment Variation[female]	0.400	0.499	0.381
Persistence Tertiary Variation[male]	0.806	0.880	0.642
Persistence Tertiary Variation[female]	0.829	0.999	0.629
Capital Elasticity Output Variation	0.425	0.478	0.279
Effect of GDP on Urban Land Requirement l Variation	1.250	1.125	0.938
Effect of GDP on Urban Land Requirement x0 Variation	5.000	5.500	6.250
Max Energy Demand per Capita Variation	0.000002	0.0000014	0.0000019
Price Elasticity of Demand Oil Variation	0.600	0.450	1.000
Price Elasticity of Demand Gas Variation	0.540	0.945	0.638
Price Elasticity of Demand Coal Variation	0.890	0.801	1.250
Price Elasticity of Demand Wind and Solar Variation	1.000	1.250	0.500
Price Elasticity of Demand Biomass Variation	0.800	0.800	1.200
Reference Change in Fossil Fuel Market Share Variation	1.000	1.800	2.200
Reference Change in Market Share Solar Variation	8.000	8.125	1.000
Reference Change in Market Share Wind Variation	6.000	2.250	1.000
Reference Change in Market Share Biomass Variation	3.250	5.250	6.000
Relative Productivity of Investment in Fossil Fuel Production Compared to Exploration Variation	10	10	10
Relative Productivity of Investment in Oil Exploration Variation	1.000	0.500	0.800
Relative Productivity of Investment in Gas Exploration Variation	1.250	0.938	1.438
Relative Productivity of Investment in Coal Exploration Variation	0.150	0.113	0.173
Effectiveness of Investment in Oil Recovery Technology Variation	2.8E-11	1.4E-11	2.24E-11
Effectiveness of Investment in Gas Recovery Technology Variation	3E-11	1.65E-11	1.95E-11
Effectiveness of Investment in Coal Recovery Technology Variation	1.3E-12	9.75E-13	1.5E-12
Solar Conversion Efficiency Factor Final Change Rate Variation	2.000	2.300	1.500
Fraction for Wind and Solar Learning Curve Strength Variation	0.200	0.230	0.140
Renewable Cost Reduction and Technology Improvement Ramp Period Variation	50.000	42.500	65.000
Fraction of Oil Revenues Invested in Technology Variation	0.040	0.020	0.032
Fraction of Gas Revenues Invested in Technology Variation	0.040	0.030	0.034
Fraction of Coal Revenues Invested in Technology Variation	0.350	0.263	0.403
Investment in Fossil Fuel Exploration and Production Delay Variation	5.000	6.250	4.250
Undiscovered Coal Resources Variation	9.00E+05	6.75E+05	1.04E+06
Annual Change in Oil Reserves Variation	2.10E+10	1.05E+10	1.68E+10

Annual Growth in Gas Reserves Variation	5000	2750	3250
Reference Cost of Solar Energy Production Final Change Rate Variation	10.000	6.000	17.500
Reference Cost of Biomass Energy Production Final Change Rate Variation	3.00E+07	1.05E+07	3.00E+06
Desired Total C Emission from Fossil Fuels Variation	7.50E+09	0.00E+00	1.00E+10
CCS Scenario Variation	0.000	1.000	0.000
Fraction of Agricultural Land Conversion from Forest Variation	0.950	0.903	1.000
Forest to Agriculture Land Allocation Time Variation	5.000	5.500	4.500
Reference meat yield Variation	0.070	0.088	0.053
Reference Input Neutral TC in Agriculture Variation	0.300	0.345	0.225
Feed Share of Grains Variation	1.000	0.500	1.500
Waste Fraction PasMeat CropMeat Variation	1.000	0.900	1.050
Waste Fraction EggsDairy Variation	1.000	0.900	1.050
Waste Fraction PlantFood Variation	1.000	0.900	1.050
Reference Daily Caloric Intake Variation	1655.800	1555.518	1756.230
Normal Shift Fraction from Vegetarianism to Meat Variation	0.010	0.005	0.007
Normal Shift Fraction from Meat to Vegetarianism Variation	0.003	0.005	0.002
Normal Fraction Intended to Change Diet Variation	0.040	0.042	0.042
Self Efficacy Multiplier Female Variation	1.200	1.500	1.080
Diet Composition Variation	0	4	0
SSP Demographic Variation Time	5	10	10
SSP Economic Variation Time	5	10	10
SSP Energy Demand Variation Time	5	10	10
SSP Energy Technology Variation Time	5	10	10
SSP Energy Production Variation Time	5	10	10
SSP Land Use Change Variation Time	5	10	10
SSP Food and Diet Variation Time	5	10	10
RCP Scenario	3	1	4
Climate Policy Scenario	0	1	0
Carbon Price Slope	5	6	0
Climate Action Year	2020	2025	2100
Land Mitigation Policy Multiplier	0.5	0.07	0
Reference CO2 Removal Rate	3.70E+07	1.75E+07	0.00E+00

References

1 Meadows, D., Richardson, J. & Bruckmann, G. *Groping in the dark: the first decade of global modelling*. (John Wiley & Sons, 1982).

2 Rydzak, F., Obersteiner, M. & Kraxner, F. Impact of Global Earth Observation-Systemic view across GEOSS societal benefit area. *International Journal of Spatial Data Infrastructures Research*, 216-243 (2010).

3 Obersteiner, M., Rydzak, F., Fritz, S. & McCallum, I. in *The Value of Information* 67-90 (Springer, 2012).

4 Walsh, B. J. *et al.* New feed sources key to ambitious climate targets. *Carbon balance and management* **10**, 26 (2015).

5 Walsh, B. *et al.* Pathways for balancing CO2 emissions and sinks. *Nature Communications* **8**, 14856 (2017). https://doi.org:10.1038/ncomms14856

6 Eker, S., Reese, G. & Obersteiner, M. Modelling the drivers of a widespread shift to sustainable diets. *Nature Sustainability* **2**, 725-735 (2019). https://doi.org:10.1038/s41893-019-0331-1

7 Moallemi, E. A. *et al.* Early systems change necessary for catalyzing long-term sustainability in a post-2030 agenda. *One Earth* **5**, 792-811 (2022). https://doi.org:https://doi.org/10.1016/j.oneear.2022.06.003

8 Liu, Q. *et al.* Robust strategies to end global poverty and reduce environmental pressures. *One Earth* **6**, 392-408 (2023). https://doi.org:https://doi.org/10.1016/j.oneear.2023.03.007

9 Rydzak, F., Obersteiner, M., Kraxner, F., Fritz, S. & McCallum, I. FeliX3 – Impact Assessment Model: Systemic view across Societal Benefit Areas beyond Global Earth Observation. (International Institute for Applied Systems Analysis (IIASA), Laxenburg, 2013).

10 Lutz, W., Goujon, A., Kc, S., Stonawski, M. & Stilianakis, N. *Demographic and human capital scenarios for the 21st century: 2018 assessment for 201 countries*. (Publications Office of the European Union, 2018).

11 World Bank. *GDP per capita (current US$)*, <https://data.worldbank.org/indicator/NY.GDP.PCAP.CD?name_desc=false> (2020).

12 United Nations. World Population Prospects 2022. (2022).

13 Bressler, R. D., Moore, F. C., Rennert, K. & Anthoff, D. Estimates of country level temperature-related mortality damage functions. *Scientific Reports* **11**, 20282 (2021). https://doi.org:10.1038/s41598-021-99156-5

14 FAO. (Food and Agriculture Organization of the United Nations, 2020).

15 Butz, W. P., Lutz, W. & J, S. *Education and differential vulnerability to natural disasters*. Special Issue, Ecology and Society edn, Vol. 19 (Resilience Alliance, 2014).

16 Lutz, W., Muttarak, R. & Striessnig, E. Universal education is key to enhanced climate adaptation. *Science* **346**, 1061-1062 (2014). https://doi.org:10.1126/science.1257975

17 Striessnig, E., Lutz, W. & Patt, A. G. Effects of educational attainment on climate risk vulnerability. *Ecology and Society* **18**, 16 (2013). https://doi.org:10.5751/ES-05252-180116

18 Lopez, A. D. & Murray, C. C. The global burden of disease, 1990–2020. *Nature medicine* **4**, 1241-1243 (1998).

19 Hughes, B. B. International Futures (IFs) economic model documentation. (2015). <https://pardee.du.edu/sites/default/files/Economics%20Documentation%20v43%20clean.pdf>.

20 Zellner, A., Kmenta, J. & Dreze, J. Specification and estimation of Cobb-Douglas production function models. *Econometrica: Journal of the Econometric Society*, 784-795 (1966). https://doi.org:10.2307/1910099

21 Nordhaus, W. Accompanying Notes and Documentation on Development of DICE-2007 Model: Notes on DICE-2007. delta. v8 as of September 21, 2007. *Miscellaneous publication, Yale University, New Haven, NE* (2007).

22 Nordhaus, W. D. Revisiting the social cost of carbon. *Proceedings of the National Academy of Sciences* **114**, 1518-1523 (2017).
23 Dietz, S. & Stern, N. Endogenous growth, convexity of damage and climate risk: how Nordhaus' framework supports deep cuts in carbon emissions. *The Economic Journal* **125**, 574-620 (2015).
24 Weitzman, M. L. GHG targets as insurance against catastrophic climate damages. *Journal of Public Economic Theory* **14**, 221-244 (2012).
25 Kalkuhl, M. & Wenz, L. The impact of climate conditions on economic production. Evidence from a global panel of regions. *Journal of Environmental Economics and Management* **103**, 102360 (2020).
26 Burke, M., Hsiang, S. M. & Miguel, E. Global non-linear effect of temperature on economic production. *Nature* **527**, 235-239 (2015). https://doi.org:10.1038/nature15725
27 Fosu, A. K. Inequality, income, and poverty: Comparative global evidence. *Social Science Quarterly* **91**, 1432-1446 (2010). https://doi.org:10.1111/j.1540-6237.2010.00739.x
28 Lakner, C., Mahler, D. G., Negre, M. & Prydz, E. B. How much does reducing inequality matter for global poverty? *The Journal of Economic Inequality*, 1-27 (2022). https://doi.org:https://doi.org/10.1007/s10888-021-09510-w
29 Soergel, B., Kriegler, E., Bodirsky, B. L., Bauer, N., Leimbach, M. & Popp, A. Combining ambitious climate policies with efforts to eradicate poverty. *Nature communications* **12**, 1-12 (2021). https://doi.org:https://doi.org/10.1038/s41467-021-22315-9
30 Cuaresma, J. C., Fengler, W., Kharas, H., Bekhtiar, K., Brottrager, M. & Hofer, M. Will the Sustainable Development Goals be fulfilled? Assessing present and future global poverty. *Palgrave Communications* **4**, 29 (2018). https://doi.org:10.1057/s41599-018-0083-y
31 Lopez, J. H. & Servén, L. *A normal relationship?: poverty, growth, and inequality*. Vol. 3814 (World Bank Publications, 2006).
32 Kemp-Benedict, E. Income distribution and poverty: methods for using available data in global analysis. *PoleStar Technical Notes* (2001).
33 Kot, S. M. Estimates of the world distribution of personal incomes based on country sample clones. (GUT FME Working Paper Series A, 2016).
34 Mendez Ramos, F. Uncertainty in Ex-Ante Poverty and Income Distribution: Insights from Output Growth and Natural Resource Country Typologies. *World Bank Policy Research Working Paper* (2019). https://doi.org:10.1596/1813-9450-8841
35 Kakwani, N. C. *Income inequality and poverty*. (World Bank, 1980).
36 Chotikapanich, D., Valenzuela, R. & Rao, D. P. Global and regional inequality in the distribution of income: estimation with limited and incomplete data. *Empirical Economics* **22**, 533-546 (1997). https://doi.org:10.1007/BF01205778
37 Dixon, P. M., Weiner, J., Mitchell-Olds, T. & Woodley, R. Bootstrapping the Gini coefficient of inequality. *Ecology* **68**, 1548-1551 (1987). https://doi.org:10.2307/1939238
38 Gastwirth, J. L. The estimation of the Lorenz curve and Gini index. *The Review of Economics and Statistics*, 306-316 (1972). https://doi.org:10.2307/1937992
39 OECD. *Education and earnings*, <https://stats.oecd.org/Index.aspx?DataSetCode=EAG_EARNINGS > (2023).
40 Mincer, J. Human capital and the labor market: A review of current research. *Educational researcher* **18**, 27-34 (1989).
41 Skirbekk, V. Age and individual productivity: A literature survey. *Vienna yearbook of population research*, 133-153 (2004).
42 Harkness, S. & Waldfogel, J. in *Worker well-being and public policy* Vol. 22 369-413 (Emerald Group Publishing Limited, 2003).
43 Bar-Haim, E., Chauvel, L., Gornick, J. C. & Hartung, A. The persistence of the gender earnings gap: Cohort trends and the role of education in twelve countries. *Social Indicators Research* **165**, 821-841 (2023). https://doi.org:https://doi.org/10.1007/s11205-022-03029-x

44 Lutz, W. *et al.* Years of good life is a well-being indicator designed to serve research on sustainability. *Proceedings of the National Academy of Sciences* **118** (2021). https://doi.org:10.1073/pnas.1907351118
45 Matson, P., Clark, W. C. & Andersson, K. *Pursuing Sustainability: A Guide to the Science and Practice*. (Princeton University Press, 2016).
46 Desai, M., Sen, A. & Boltvinik, J. *Social Progress Index: A Proposal*. (United Nations Development Programme, 1992).
47 Sullivan, D. F. A single index of mortality and morbidity. *HSMHA Health Rep* **86**, 347-354 (1971).
48 Aanegola, R., Sakai, S. N. & Kumar, N. Longitudinal analysis of the determinants of life expectancy and healthy life expectancy: A causal approach. *Healthcare Analytics* **2**, 100028 (2022).
49 Riahi, K. *et al.* The Shared Socioeconomic Pathways and their energy, land use, and greenhouse gas emissions implications: An overview. *Global Environmental Change* **42**, 153-168 (2017). https://doi.org:https://doi.org/10.1016/j.gloenvcha.2016.05.009
50 Huppmann, D., Rogelj, J., Kriegler, E., Krey, V. & Riahi, K. A new scenario resource for integrated 1.5 °C research. *Nature Climate Change* **8**, 1027-1030 (2018). https://doi.org:10.1038/s41558-018-0317-4
51 Burgess, M. G., Langendorf, R. E., Moyer, J. D., Dancer, A., Hughes, B. B. & Tilman, D. Multidecadal dynamics project slow 21st-century economic growth and income convergence. *Communications Earth & Environment* **4**, 220 (2023). https://doi.org:10.1038/s43247-023-00874-7
52 Moyer, J. D. Blessed are the peacemakers: The future burden of intrastate conflict on poverty. *World Development* **165**, 106188 (2023). https://doi.org:https://doi.org/10.1016/j.worlddev.2023.106188